



# The role of thermokarst evolution in debris flow initiation (Hüttekarr Rock Glacier, Austrian Alps)

Simon Seelig<sup>1</sup>, Thomas Wagner<sup>1</sup>, Karl Krainer<sup>2</sup>, Michael Avian<sup>3</sup>, Marc Olefs<sup>3</sup>, Klaus Haslinger<sup>3</sup>, and Gerfried Winkler<sup>1</sup>

<sup>1</sup>Institute of Earth Sciences, NAWI Graz Geocenter, University of Graz, Heinrichstrasse 26, 8010 Graz, Austria

<sup>2</sup>Institute of Geology, University of Innsbruck, Innrain 52, 6020 Innsbruck, Austria

<sup>3</sup>Central Institute for Meteorology and Geodynamics, Hohe Warte 38, 1190 Vienna, Austria

**Correspondence:** Simon Seelig (simon.seelig@uni-graz.at)

**Abstract.** A rapid sequence of cascading events involving thermokarst lake outburst, rock glacier front failure, debris flow development and river blockage hit Radurschl Valley (Ötztal Alps, Tyrol) on 13 August 2019. Compounding effects from multivariate permafrost degradation and drainage network development initiated the complex process chain. The debris flow dammed the main river of the valley, impounding a water volume of 120,000 m<sup>3</sup> that was partly drained by excavation to prevent a potentially catastrophic outburst flood. Since the environmental forces inducing the debris flow evolved under ambiguous conditions, potentially destabilizing factors were analyzed systematically to deduce the failure mechanism and establish a basis for multi hazard assessment in similar settings. Identification and evaluation of individual factors revealed a critical combination of topographical and sedimentological disposition, climate, and weather patterns driving the evolution of thermokarst and debris flow. Progressively changing groundwater flow and storage patterns characterizing the hydraulic configuration within the frozen sediment accumulation governed the slope stability of the rock glacier front. The large amount of mobilizable sediment, dynamically changing internal structure, and substantial water flow along a rapidly evolving channel network eroded into the permafrost body, render active rock glaciers complex multi hazard elements in periglacial, mountainous environments.

## 1 Introduction

Climate change and its adverse effects on slope stability rapidly alter patterns of landslide occurrence and the balance between destabilizing and resisting forces (Crozier, 2010; Gariano and Guzzetti, 2016; Adler et al., 2022). Landslide engineers and decision makers face a delicate challenge since data-driven hazard assessment methods are at risk of losing predictive power as boundary conditions change at timescales that are short compared to typically available landslide records (Haeberli and Whiteman, 2015; Patton et al., 2019). In this context, a process-based understanding of potential failure mechanisms is indispensable for identifying landslide hazard at sites considered stable under past conditions (Evans and Delaney, 2015; Schauwecker et al., 2019). This is especially true for debris flows initiating in permafrost affected terrain, due to the rapid alteration of slope stability in their initiation zones, their ability to traverse great distances at high velocities, and their high impact forces (Jakob and Hungr, 2005; Jakob et al., 2012; Petley, 2012; Dowling and Santi, 2014; Nikolopoulos et al., 2014). Hence failure in remote



areas which are typically characterized by data scarcity and incomplete monitoring has the potential to dramatically affect people and infrastructure far from debris flow initiation (Haque et al., 2016, 2019).

25 The European Alps are affected by severe increases in surface air temperature ( $\sim 0.3$  °C per decade, exceeding global warming rates), altering snow cover dynamics and driving permafrost thaw (Beniston et al., 2018; Hock et al., 2019; Patton et al., 2019; Olefs et al., 2020; Matiu et al., 2021; Fox-Kemper et al., 2021). The increasing frequency of high-intensity precipitation events amplifies the likelihood of landslides (Giorgi et al., 2016; Rajczak and Schär, 2017; Schlögl and Matulla, 2018; Hock et al., 2019; Patton et al., 2019; Ranasinghe et al., 2021). Slope stability decreases as subsurface liquid water  
30 content, ice ductility, and permeability increase in response to permafrost degradation (Patton et al., 2019; Hock et al., 2019). Moreover, glacier retreat enhances the accumulation of loose, unstable sediment at high elevations (Stoffel and Huggel, 2012; Deline et al., 2015; Buckel et al., 2018; Hock et al., 2019; Mölg et al., 2021). These changing environmental conditions alter the geotechnical and hydraulic ground properties, and modify the characteristics and seasonality of landslides accordingly (Stoffel and Huggel, 2012; Gariano and Guzzetti, 2016; Beniston et al., 2018; Patton et al., 2019). The consecutive variation in process  
35 chains and cascading events makes them especially difficult to predict under a changing climate, with potentially catastrophic consequences downstream (Deline et al., 2015).

In terms of landslide initiation, the steep slopes and large sediment accumulations provided by active rock glacier fronts pose a serious hazard. Active rock glaciers, i. e. distinct sediment accumulations consisting of ice-debris mixtures slowly creeping downhill, constitute important periglacial landforms regarding sediment dynamics and hydrology due to their large sediment  
40 transfer capability, pronounced water storage capacity, and wide-spread occurrence in mountainous terrain (Kummert and Delaloye, 2018; Winkler et al., 2018; Jones et al., 2019b; Hayashi, 2020; Wagner et al., 2020, 2021a). Common deformation rates are on the order of decimeters to meters per year, accelerating across the European Alps in response to climate change (Kääb et al., 2007; Roer et al., 2008; Beniston et al., 2018; Groh and Blöthe, 2019; Hock et al., 2019; Kenner et al., 2020; Fleischer et al., 2021; Fox-Kemper et al., 2021; Marcer et al., 2021). Thermo–hydro–mechanical processes determine the  
45 deformation characteristics of rock glaciers, with plastic deformation governed by permafrost ice content and temperature, while discrete shear failure is commonly initiated by elevated pore-water pressures along the failure surface (Arenson and Springman, 2005; Ikeda et al., 2008; Buchli et al., 2013, 2018; Krainer et al., 2015; Cicoira et al., 2019; Kofler et al., 2021). Active rock glaciers exhibit complex drainage patterns indicating a dual groundwater flow system, where large amounts of water are rapidly transported along a network of convoluted meltwater channels eroded into the frozen rock glacier core  
50 (Wahrhaftig and Cox, 1959; Potter, 1972; White, 1971; Johnson, 1978; Giardino et al., 1991; Burger et al., 1999; Krainer and Mostler, 2002; Vonder Mühl et al., 2003; Arenson et al., 2010; Springman et al., 2012; Winkler et al., 2018; Jones et al., 2019b; Wagner et al., 2021b; Kainz, 2022).

Active rock glaciers constitute multi hazard elements (Kappes et al., 2012; Gallina et al., 2016) in that they induce a spectrum of mass movement processes ranging from occasional rockfall to debris flow events, potentially involving complex chain  
55 processes (Burger et al., 1999; Kummert and Delaloye, 2018; Kummert et al., 2018). Destabilizing rock glaciers frequently experience significant acceleration, often accompanied by the appearance of morphological discontinuities such as cracks and crevasses (Kääb et al., 2007; Roer et al., 2008; Stoffel and Huggel, 2012; Delaloye et al., 2013; Marcer et al., 2019).



Debris flows initiated by destabilizing rock glacier fronts occur most frequently in response to heavy rainfall. However, intense snowmelt, rain-on-snow events, and exceptionally warm periods have also been discerned as triggering factors (Rebetez et al., 1997; Lugon and Stoffel, 2010; Krainer et al., 2012; Bodin et al., 2017; Kummert et al., 2018; Marcer et al., 2020; Kofler et al., 2021). Regardless of the detailed initiation process, the mechanics of debris flows require excessive amounts of water, capable of transporting the mobilized debris down the flow path (Soeters and van Westen, 1996). Thus, assessing the hazard potential of rock glaciers requires an integrated approach combining hydrogeological, meteorological, thermal, geomorphological, and mechanical aspects in a coherent framework.

The aim of this paper is to explore the destabilizing factors leading to failure of an active rock glacier front in a high mountain cirque, and the actuated cascading processes involving thermokarst lake outburst flood, debris flow and river blockage. We evaluate a set of potentially contributing factors, assess critical combinations, and develop a consistent conception explaining debris flow initiation and evolution. Similarities and differences with respect to documented rock glacier front failures and glacial lake outburst floods (GLOFs) are analyzed, and conclusions drawn regarding hazard potential.

## 2 Study site

The study site comprises the highest areas of Radurschl Valley, a valley in the Western Ötztal Alps constituting a headwater tributary to the Inn River (Fig. 1). The landscape is characterized by rugged terrain of glacial and periglacial origin, including steep slopes and crests, interrupted by relatively flat areas covered by talus, moraines, and periglacial sediments. The area shows an exceptionally high rock glacier density (56 % areal coverage), as well as small remnants of cirque glaciers in its uppermost parts (Kerschner, 1982; Krainer and Ribis, 2012; Wagner et al., 2020, 2021a).

The specific cirque under consideration is the Hüttekarkirque, a small (2.8 km<sup>2</sup>) headwater catchment encircled by ragged rock walls except to the west, where it steeply descends to Radurschl Valley (Fig. 2; 46°54' N, 10°39' E). The altitudinal range in the study area varies from 2,387 to 3,353 m a. s. l. (mean altitude 2,870 m a. s. l.), including a relatively flat valley bottom between 2,600 and 2,700 m a. s. l. The bedrock lithology is composed of metamorphic rocks of the Ötztal–Stubai–Complex (Ötztal–Bundschuh nappe system; Hoinkes and Thöni (1993); Schmid et al. (2004)), as illustrated in Fig. 3. The mountain ridges bordering the cirque to the south and to the east are dominated by orthogneiss (augen- and flasergneiss), the ridge to the north and northwest exhibits muscovite-granite-orthogneiss. At Rotschragenjoch and south of Bruchkopf, paragneiss and micaschist with thin intercalations of amphibolite are exposed. The terrain is composed of bedrock (38 %) mainly exposed in the highest parts, talus, and debris slopes (17 %) along the valley sides, while the lower parts are covered by moraine deposits (12 %) and four rock glaciers (27 %). Two small, north facing cirque glaciers (Glockturmferner, Hüttekarkirque; 6 %) are situated at 2,853 and 3,029 m a. s. l., respectively.

The local climate is influenced by the dry, inner alpine conditions prevailing in the Ötztal Alps (Frei and Schär, 1998; Isotta et al., 2014). Moderate annual precipitation (1042 mm) and low mean annual air temperature (-2.5 °C) reflect the high altitude of Hüttekarkirque and its central position close to the main chain of the Alps. Monthly precipitation reaches its maximum in August and its minimum in February, with the respective months corresponding to the highest and lowest mean air temperature

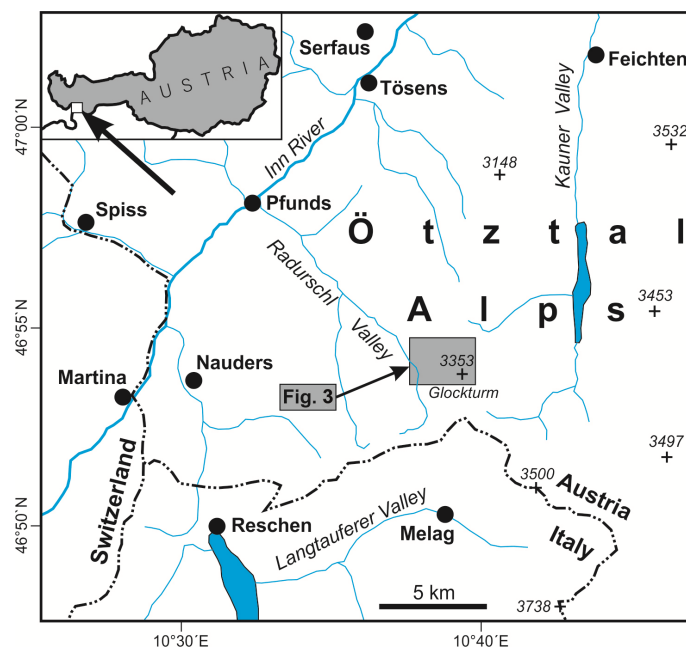


**Figure 1.** Location map of Hüttekär in the Ötztal Alps, Tyrol (Austria).

**Table 1.** Long-term (1976–2019) mean monthly air temperature and precipitation in Hüttekär-cirque (based on Hiebl and Frei (2016, 2018)).

	J	F	M	A	M	J	J	A	S	O	N	D
Air temperature (°C)	-9.7	-9.8	-7.7	-4.9	-0.3	3.2	5.4	5.4	2.3	-0.5	-5.5	-8.4
Precipitation (mm)	64	45	61	57	99	125	151	156	90	71	61	62

(Table 1). The local altitude distribution and dry climatic conditions promote the development of rock glaciers. The equilibrium line altitude of glaciers, rising from ~3,100 to ~3,300 m a. s. l. during the 20<sup>th</sup> century, is located within the steep summit region (Žebre et al., 2021). These unfavorable conditions for cirque glacier development allow rock glaciers to cover the extensive flat terrain above the lower permafrost boundary, ranging from ~2,400 to ~2,600 m a. s. l. (Kerschner, 1982; Boeckli et al., 2012a; Ribis, 2017).

The coevolution of cirque glaciers and rock glaciers is highlighted by comparing a set of glacier inventories ranging from the little ice age (about 1850 CE) to 2015 CE (Fig. S1; Fischer et al. (2015); Buckel et al. (2018)), documenting the development of Glockturnferner from a pure ice glacier to a largely debris covered glacier, presumably transitioning into the ice-cored rock glacier below (Anderson et al., 2018; Jones et al., 2019a; Knight et al., 2019). Along the surface of Hüttekär Rock Glacier, distinct ridges and furrows are visible in the northernmost part, while the central and southern parts show a smooth and flat surface morphology. Rock glacier debris is composed of orthogneiss derived from the Glockturn massif. Poorly sorted boulders, arranged in a loose, clast-supported structure form a heterogeneous surface layer of variable thickness. The blocky

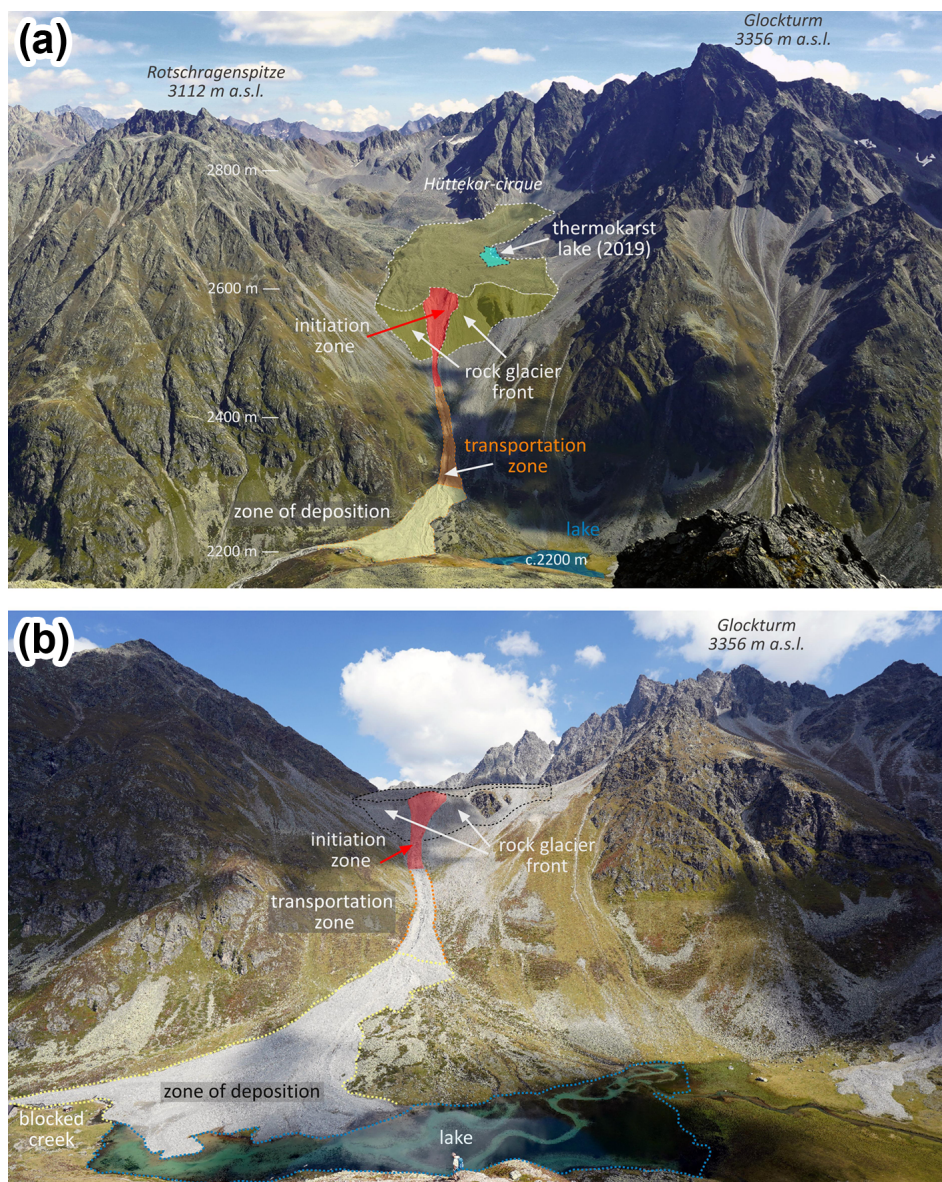


**Figure 2.** (a) Illustration of Hüttekarcirque, Hüttekarcirque Rock Glacier, the debris flow and the impounded lake (view is towards the east). The debris flow was initiated at the steep front of Hüttekarcirque Rock Glacier (highlighted), caused by rapid drainage of a thermokarst lake that existed between 01 June and 13 August 2019 (former position indicated). The debris flow path sections are outlined and labelled according to Hungr (2005). (b) Debris flow morphology two years after its initiation. The progressively enlarging initiation zone eroded already significant parts of the steep rock glacier front. The transport zone is characterized by a set of levees along a narrow channel. The former flow path of the blocked river is still clearly visible below the lake surface. The channel draining the lake was excavated to prevent a potentially catastrophic outburst following river blockage in August 2019 (photographs: Rudolf Philippitsch, 14 September 2021).

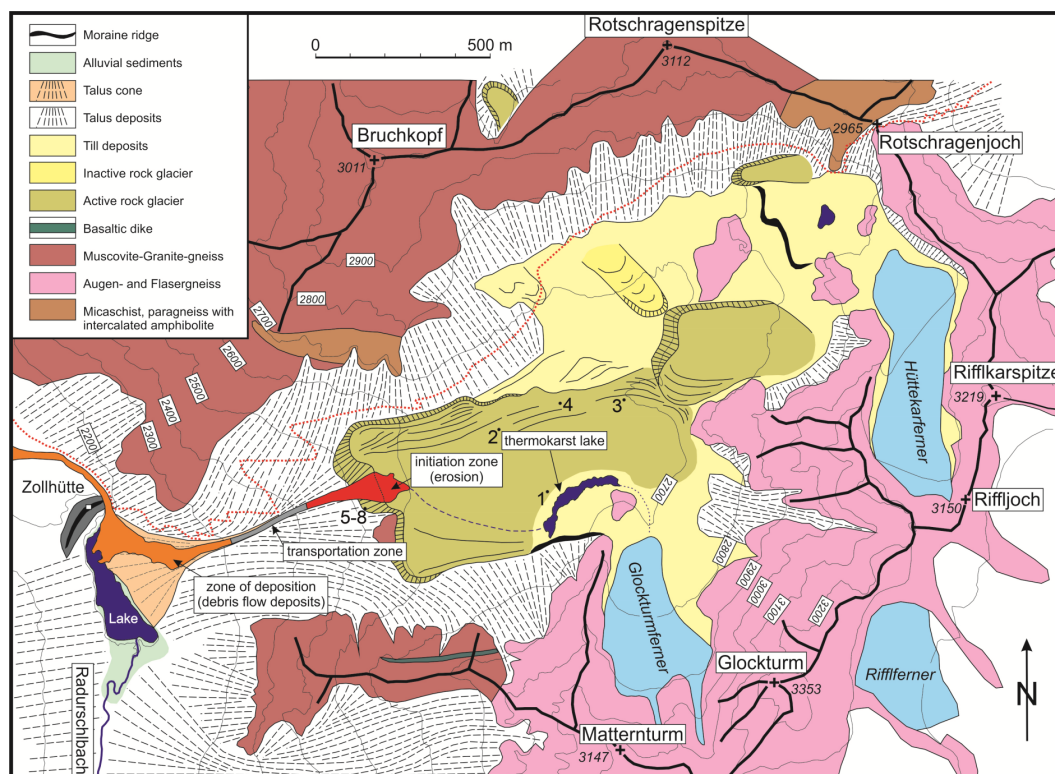


**Figure 3.** Geological-geomorphological map, compiled using the most recent provisional geological map provided by the Geological Survey of Austria (Moser, 2012). It is complemented by ortho-images and a high-resolution digital terrain model (DTM) derived from airborne laser scanning data (Government of the Province of Tyrol, 2021a). The preliminary map is based on comprehensive field mapping (2019–2021). Numbers indicate grain size analysis sampling locations.

surface layer covers a finer-grained, frozen layer dominated by well-graded gravel and sand that is exposed along the rock glacier front. Water flowing along the permafrost table is visible and audible between boulders at several places in the southern part of the rock glacier, following distinct channels eroded into the ice core. Despite its considerable catchment area, Hüttekarcirque is drained exclusively by subsurface flow, emerging as a group of small springs at the toe of the slope descending to Radurschltal.

### 3 Debris flow event

An active, retrogressive debris flow erodes the steep slope bordering Hüttekarcirque to the west (Fig. 2; classification according to Varnes (1978); Cruden and Varnes (1996); Hungr et al. (2014)). Following a moderate precipitation event, destabilization initiated on 13 August 2019, mobilizing a volume of several thousand m<sup>3</sup> from the steep rock glacier front (Fig. 4a). The event description is based on in situ observations of Josef Waldner, staff of the nearby hut Hohenzollernhaus (pers. comm.).



The debris flow started at 03:00 AM (Central European Summer Time, UTC+2), the main event lasted until about 12:00 PM, followed by reduced debris flow activity that persisted until the next day. Slope failure initiated along an irregularly shaped  
115 rupture in ice-cemented debris, exposed at the main scarp (Fig. 4b). Accelerating and disintegrating, the transported mass evolved into a debris flow following a narrow channel down the steep slope below the rock glacier front (Fig. 2, Fig. 3). About 200 m below the initiation zone, the material spread out and formed a deposition fan of 33,000 m<sup>2</sup> and an estimated volume of 40,000 – 50,000 m<sup>3</sup>, thereby damming the river Radurschlbach at 2,200 m a. s. l. (Fig. 4c, Fig. 4d). Consequently, a lake covering an area of ~60,000 m<sup>2</sup> developed in Radurschl Valley, causing the downstream riverbed to fall dry temporarily (Fig.  
120 4c). Excavation of a drainage channel lowered the mean water depth from 2 m to 1 m during the following days to prevent a potentially catastrophic outburst. Subsequently, a dam was constructed on the debris fan to restrain future debris flows from damming Radurschlbach again.

Concurrently with the debris flow initiation, a thermokarst lake on top of Hüttekark Rock Glacier (~350 m behind the initiation zone; Fig. 3, Fig. 4e, Fig. 4f) drained almost completely within one day. The thermokarst lake had started to develop  
125 coincidentally with the onset of snowmelt in early June 2019 within a shallow depression where massive ice within the rock glacier prevented drainage (Fig. 4g). During the last decades, a comparable feature had never been observed before in Hüttekark-cirque, despite frequent visits by hikers, hunters, shepherds, and staff of Hohenzollernhaus. In the stage of its largest extent, the thermokarst lake was approximately 300 m long, up to about 150 m wide and 4–5 m deep, comprising an estimated water volume of ~150,000 m<sup>3</sup>. Effective drainage through a large crevasse (width ~1.5 m, height ~2 m) caused initiation of the  
130 debris flow at the front of the rock glacier (Fig. 4e, Fig. 4f, Fig. 4h). Large amounts of water were rapidly transferred to the debris flow initiation zone and torrent beneath. Retrogressive linear erosion visible in the initiation zone indicates that concentrated water flow emerged at the main scarp (Fig. 4b), in good agreement with earlier observations of rock glacier front failures (Kummert et al., 2018; Marcer et al., 2020; Kofler et al., 2021). Since then, the depression never filled again but still shows distinct morphology.

#### 135 4 Methods

The inherent stability of the slope under consideration determines its response to changes affecting the balance of driving and resisting forces (Glade and Crozier, 2005; Crozier, 2010). Systematic identification of factors promoting slope instability is conducted by differentiating (Glade and Crozier, 2005):

- (1) predisposing factors (inducing a static setting capable of enhancing the destabilizing impact of dynamic forces),
- 140 (2) preparatory factors (dynamic forces shifting the slope towards a state susceptible to failure), and
- (3) triggering factors (dynamic forces initiating failure).

Acknowledging that debris flow hazard analysis requires consideration of multiple destabilizing factors, their impact on slope stability is characterized individually to establish a basis for reconstructing the failure mechanism. The chosen methods aim at maximizing comparability to earlier studies on rock glacier front failures and debris flows in periglacial regions.

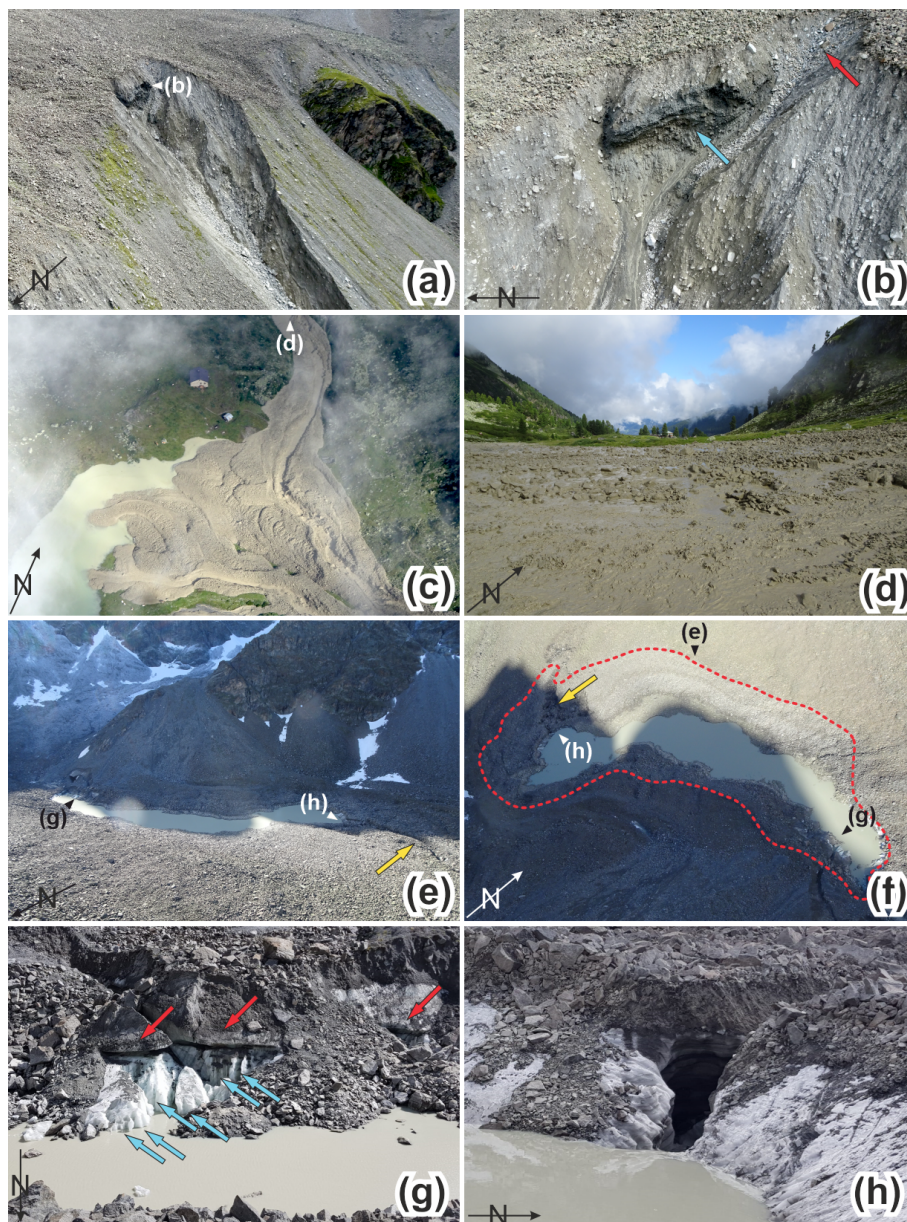


**Figure 4.** Images documenting the debris flow event that initiated on 13 August 2019. (a) Debris flow initiation zone at the steep front of Hüttekarak Rock Glacier. (b) Ice-cemented debris (blue arrow) exposed in the main scarp. Linear retrogressive erosion indicates concentrated water flow (red arrow). (c) Debris flow deposits blocking Radurschbach. (d) Debris flow material. (e) Thermokarst lake and drainage channel (yellow arrow) on Hüttekarak Rock Glacier. (f) Extent of thermokarst lake on 14 August 2019 and maximum extent one day earlier (dashed line). The channel connecting the lake to the debris flow initiation zone is indicated by the yellow arrow. (g) Impermeable ice underlying the thermokarst lake. Blue arrows indicate vertical convexities attributed to thermal convection of water during the lake development. Red arrows indicate undercutting of the ice along the lake shoreline, promoted by thermal convection. (h) Thermokarst channel eroded into the frozen rock glacier core, facilitating rapid drainage of the thermokarst lake. Photographs were taken on 14 August 2019 (c–h) and 26 August 2019 (a–b), respectively, by Roman Außerlechner, Thomas Figl, Werner Thöny, and Josef Waldner.



#### 145 4.1 Predisposing factor analysis

A topographical setting promoting rock glacier destabilization is a necessary (but not sufficient) precondition for rock glacier front failure. Attributes significantly affecting slope stability include morphometric parameters such as length, slope angle, and curvature (Chowdhury et al., 2010; Reichenbach et al., 2018; Marcer et al., 2019). Sediment erosion, transport, and deposition depend on local energy gradients, available transport vectors, and material properties (Bracken et al., 2015). Collectively, these variables control local loading stresses and the availability of material for subsequent mobilization (Kummert et al., 2018; Kofler et al., 2021). The respective impact of these factors on slope stability is evaluated using a high-resolution ( $1 \times 1$  m) DTM based on airborne laserscanning data acquired two years prior to debris flow occurrence (Government of the Province of Tyrol, 2021a), applying SAGA GIS 2.1.4 for morphometric analyses (Conrad et al., 2015). Slope angle and downslope curvature calculations (Freeman, 1991) are performed using a smoothed (cubic convolution resampling to  $10 \times 10$  m) DTM to detect the fundamental topographical features.

Thermal ground conditions and the presence of subsurface ice affect the shear strength of involved materials, alter groundwater flow patterns, and impact the storage and release of water by thermokarst evolution. The spatial permafrost distribution is estimated by taking recourse to the Alpine Permafrost Index Map, providing a static proxy for potential permafrost occurrence and its spatial coherence (Boeckli et al., 2012b, a). While the dynamic effect of climate change is not considered explicitly by the index map, permafrost degradation is expected to intensify close to the lower permafrost boundary (Marcer et al., 2019). The local influence of topography on the energy available for permafrost degradation (Scherler et al., 2014; Marcer et al., 2019) is assessed by calculating the potential incoming solar radiation based on the DTM (Hock, 2005; Cuffey and Paterson, 2010). Calculations of mean annual solar radiation under clear-sky conditions are performed employing GRASS GIS 8.0 (GRASS Development Team, 2022) module r.sun (Hofierka et al., 2007), assuming an average surface albedo of 0.2.

The mechanics of debris flows are largely determined by solid-fluid interactions, rendering grain size distribution and water content major variables driving flow behavior (Iverson, 1997). The rate of water supply is determined by the permeability of sediments above the initiation zone. Geotechnical and hydrogeological characteristics of the materials involved are inspected by analyzing the grain size distribution of the rock glacier surface layer at one coarse-grained and three relatively fine-grained domains (sampling locations indicated in Fig. 3). At each location the maximum diameter of 200 clasts lying side by side is measured in an area of approximately  $2 \times 2$  m (fine grained domains) to  $5 \times 5$  m (coarse grained domain). The grain size distribution of the poorly sorted sediment layer below the blocky surface is analyzed by manual wet sieving of a sample taken at the steep rock glacier front.

#### 4.2 Preparatory factor analysis

The geometry of the active rock glacier front depends on the dynamic balance between rock glacier kinematics and erosion rates (Kummert and Delaloye, 2018). Time series of ortho-images are used to quantify rock glacier surface displacement rates and the evolution of surface features indicating destabilization (including cracks, crevasses, and scarps; Avian et al. (2007); Roer et al. (2008); Delaloye et al. (2013); Marcer et al. (2019); ortho-images provided by the Government of the Province



of Tyrol (2021b)). In the observation period 1970–2020, 200 prominent blocks, geometrically well distributed on the rock glacier surface, are visually identified at each ortho-image epoch to approximate the horizontal surface displacement rate at the respective location. Additionally, the position of the rock glacier front line (top of the erosional slope) is mapped at every epoch. Both analyses provide the basis for assessing the kinetic patterns on the rock glacier surface (Avian et al., 2009; Kummert and Delaloye, 2018).

Climatic factors and their progressive change exert a key control on slope stability (Gariano and Guzzetti, 2016; Patton et al., 2019). Alterations in volume and intensity of rainfall, snowmelt and ice melt affect subsurface water content, pore-water pressure and seepage forces (Ikeda et al., 2008; Cicoira et al., 2019; Patton et al., 2019). The long-term evolution of air temperature and precipitation in Hüttekarakirque is evaluated using the gridded (1 × 1 km) SPARTACUS data set (Spatiotemporal Reanalysis Dataset for Climate in Austria; Hiebl and Frei (2016, 2018)). Daily precipitation totals and 24 hour mean air temperature data observed from 1976 to 2019 are extracted and averaged across Hüttekarakirque. Specific aspects of the local climate are explored by calculating the annual positive degree day sum (daily mean air temperature > 0 °C) as proxy for available melting energy, as well as precipitation due to very wet days (> 95<sup>th</sup> percentile) reflecting the annual magnitude of heavy precipitation events (Klein Tank et al., 2009; Cuffey and Paterson, 2010). Considering that the hydrometeorological conditions preceding the debris flow determine the critical amount of water necessary to initiate failure (Crozier, 2010), the impact of these climate indices is assessed by comparing their respective values during summer 2019 (01 June–13 August) to previous years (1976–2019). To estimate changes in their central tendency, trend direction and rate of change are evaluated using the nonparametric seasonal Mann Kendall test (Theil, 1950; Sen, 1968; Hirsch et al., 1982; Hirsch and Slack, 1984). Calculations are performed employing R packages 'rkt' 1.6 (Marchetto, 2021) and 'climdex.pcic' 1.1 (Bronaugh, 2020), implemented in R 4.2.0 (R Core Team, 2022).

In the Alps, individual storms exhibit strong intensity gradients at length scales < 5 km (i. e. below the basic length-to-crest scale; Haiden et al. (2011); Nikolopoulos et al. (2014, 2015a); Marra et al. (2016); Destro et al. (2017)). The combination of weather station data and remote sensing information allows the detection of individual event characteristics (Haiden et al., 2011; Borga et al., 2014; Marra et al., 2014, 2016; Destro et al., 2017). Detailed (~hourly) temporal resolution of precipitation data is necessary to avoid biased estimates of rainfall intensity and duration (Marra, 2019). Meteorological analyses at time intervals from hours to months are thus based on the INCA system (Integrated Nowcasting through Comprehensive Analysis; Haiden et al. (2011)), providing gridded (1 × 1 km) data sets at hourly temporal resolution. Inclusion of 12 weather stations at a distance < 25 km from Hüttekarakirque, in combination with C-band radar measurements and Meteosat Second Generation Satellite Products, allows assessing the spatial and temporal patterns of meteorological conditions at the study site.

Snow cover development is assessed using the spatially distributed, physically based snow cover model SNOWGRID (Olefs et al., 2013). It employs a simple two-layer scheme, considering settling, the heat and liquid water content of the snow cover, snowline depression effects and the energy added by rain. For every time step and layer, the state variables snow density, snow water equivalent, snow temperature, liquid water content, bottom liquid water flux, and surface albedo are calculated. The primary focus of the model is to obtain a high-resolution representation of their spatial distribution and to provide fast calculations on a large grid. The model employs a 100 × 100 m bilinear interpolation of the INCA data set in combination with



schemes for radiation and cloudiness developed at the Central Institute for Meteorology and Geodynamics (Austria). These are based on ground measurements, satellite products, and high quality solar and terrestrial radiation data (Olefs et al., 2013, 2016).  
215 For each winter season, the cumulated snowmelt volume in Hüttekarcirque is calculated and compared to the 2018/19 season. The rate of snowmelt is approximated by the respective seasonal average during the time span between maximal snow volume and complete ablation of the winter snow cover (Kofler et al., 2021).

Glacial meltwater infiltrates directly from Glockturnferner and indirectly from Hüttekarcirque into the rock glacier (Fig. 3), thus the total volume and average rate of ice melt is calculated for each year between ablation of the snow cover and 13 August, based on the surface energy balance for the respective glacier (Hock, 2005; Cuffey and Paterson, 2010). Ice melt rates  
220 are calculated at hourly intervals by evaluating radiative, turbulent and advective energy fluxes per glacier derived from INCA, assuming a constant glacier surface temperature of 0 °C (considered a reasonable approximation for the ablation zones of temperate glaciers during the summer season; Cuffey and Paterson (2010)). Shortwave net radiation is calculated by evaluating global radiation, accounting for the reflective and shadowing influences of topography as outlined in Sect. 4.1. Atmospheric  
225 conditions influencing longwave radiation are considered following Greuell et al. (1997) and Oerlemans (2000). Sensible and latent heat fluxes are calculated by parameterization of the respective transport processes based on turbulence similarity (Cuffey and Paterson, 2010). The rainfall heat flux is estimated assuming that rainfall temperature approaches the near-surface air temperature. Physical specifications and plausibility evaluation are provided in Appendix A.

### 4.3 Triggering factor analysis

Rainfall-induced debris flows are triggered by infiltration rates exceeding subsurface drainage rates and the corresponding alteration of pore-water pressures (Sidle, 1984; Johnson and Sitar, 1990; Anderson and Sitar, 1995; Wieczorek, 1996; Wieczorek and Glade, 2005; Crozier, 2010). Infiltrating water adversely affects slope stability by adding additional weight while simultaneously decreasing shear strength, either by lowering effective stresses in response to increasing positive pore-water pressures or by eliminating suction due to declining negative pore-water pressures (Johnson and Sitar, 1990; Anderson and Sitar, 1995;  
235 Chowdhury et al., 2010; Crozier, 2010). In order to evaluate the impact of the storm immediately preceding the debris flow on 13 August 2019, rainfall time series are extracted from INCA, averaged across the potentially contributing area (Hüttekarcirque), and discretized into single events by defining a minimum of 24 hours between individual events (Nikolopoulos et al., 2015b; Marra et al., 2016). Calculations are performed employing the R package 'IETD' 1.0 (Duque, 2020), implemented in R 4.2.0 (R Core Team, 2022). The resulting ensemble of rainfall event duration, volume and average intensity is analyzed by  
240 conducting a frequency analysis. The severity of individual events is assessed employing the frequentist approach developed by Brunetti et al. (2010) and Peruccacci et al. (2012). The rainfall event characteristics immediately preceding the slope failure are compared to regional critical rainfall thresholds for debris flow initiation (Nikolopoulos et al., 2015b; Marra et al., 2016).

Glacial lake outbursts evolving into debris flows are commonly initiated by mechanical failure of the dam or by rapid expansion of the lake drainage system through thermal erosion of ground ice. The volume and geometry of the impounded reservoir,  
245 dam characteristics, failure mechanism, downstream topography and sediment availability control the hazard potential (Clague and Evans, 1994). The development of thermokarst features, including meltwater lakes and channels, is highly sensitive to



thermal ground conditions and their response to climate change (Kääb and Haeberli, 2001). The spatiotemporal evolution of the thermokarst lake on Hüttekar Rock Glacier is deduced by combining Sentinel-2 multi-spectral satellite data and the latest (2017/18) available DTM, characterizing the lake surface area dynamics and corresponding water volume development (modified Copernicus data 2020 processed by Sentinel Hub; Sentinel Hub (2020); Government of the Province of Tyrol (2021a)). Due to the dynamic nature of the rock glacier surface, volume estimates are considered rough estimates, failing to account for water stored in the pore space and potential intra-permafrost channels. Breakthrough of thermokarst channels is facilitated by a positive feedback mechanism of energy transfer along the channel system inducing ice melt and channel enlargement, which in turn increases discharge and accelerates channel growth (Nye, 1976; Clarke, 1982, 2003; Spring and Hutter, 1981a, b; Clague and Evans, 1994; Walder and Costa, 1996; Huggel et al., 2004; Cuffey and Paterson, 2010; Clague and O'Connor, 2015). Dimensional analysis indicates that the energy provided by the upstream water body governs expansion rates of the drainage system (Clarke, 1982, 2003; Cuffey and Paterson, 2010). The prediction of the specific channel system evolution is impossible without exact knowledge of its geometry and hydraulic properties. However, the estimation of the meltwater lake energy budget provides a measure of the total energy available for thermokarst development. Undercutting and vertical pipe structures eroded into the ice along the lake shoreline provide field evidence for thermal convection (Fig. 4g), promoting energy turnover and melting of ice beneath the lake while constraining the surface water temperature to  $< 4^{\circ}\text{C}$  due to negative thermal expansion (Haeberli et al., 2001; Kääb and Haeberli, 2001; Werder et al., 2010). Rapid transfer of energy exchanged at the lake surface to the ice sealing the lake bottom keeps the water at roughly constant temperature, thus allowing for an assessment of the lake energy balance based on INCA data (physical specifications are provided in Appendix A).

## 265 5 Results

A systematic evaluation of destabilizing factors and adverse combinations thereof requires an individual evaluation of every potentially contributing factor.

### 5.1 Predisposing factors

Morphometric analysis of the study area reveals several features promoting debris flow development. The slope (900 m long and 400 m in elevation difference) bordering Hüttekar-cirque to the west shows a very steep, convex top and a steep, concave main part (Fig. 5a, Fig. 5b). Prior to landslide initiation, the prospective initiation zone was characterized by steep slope angle and convex downslope curvature (Table 2). The channel below the rock glacier front was less steep and concave, while the debris fan was already comparatively flat before the 2019 debris flow (Table 2). Irregular micromorphology, depositional levees, and boulder trains document earlier debris flows (Fig. 2, Fig. 5; Soeters and van Westen (1996); Pack (2005); Hungr et al. (2014)). Material eroded at the rock glacier front is available for subsequent mobilization further downslope, inhibiting the formation of a stabilizing debris accumulation at the toe of the rock glacier front (Kummert and Delaloye, 2018; Kummert et al., 2018; Kofler et al., 2021).

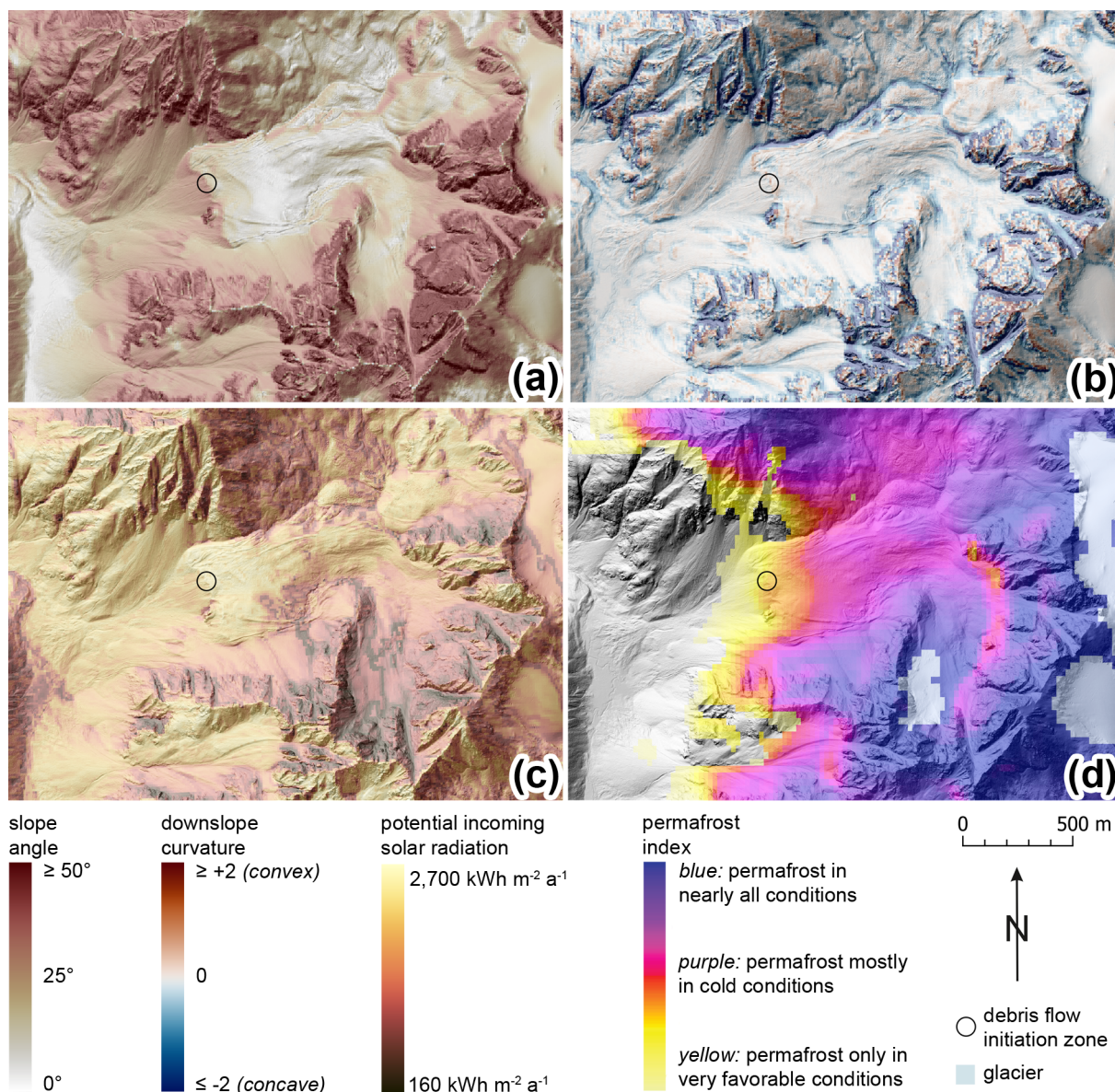


**Figure 5.** Spatial distribution of predisposing factors across Hüttekarkirque prior to debris flow initiation. (a) Slope angle, indicating that the debris flow initiated in steep terrain (33°). (b) Downslope curvature, demonstrating that convex topography prevailed in the initiation zone before the debris flow event (+0.05). (c) Potential incoming solar radiation, illustrating the high-energy environment characterizing the debris flow initiation zone (2135 kWh m<sup>-2</sup> a<sup>-1</sup>). (d) Permafrost index, indicating that the debris flow initiated close to the lower permafrost boundary (Boeckli et al., 2012a). Terrain analyses are based on a high-resolution DTM acquired in the period 2017/2018 by the Government of the Province of Tyrol (2021a). Perceptually uniform and color-vision-deficiency friendly color maps provided by Crameri (2018).



**Table 2.** Morphometric analysis based on a high-resolution DTM acquired in the period 2017/2018 by the Government of the Province of Tyrol (2021a). Results are given as averages across the debris flow initiation zone, transportation zone, and zone of deposition, respectively (indicated in Fig. 3)

Morphometric parameter	Initiation zone	Transportation zone	Zone of deposition
Mean altitude (m a.s.l.)	2,541	2,362	2,227
Mean slope gradient (°)	33.0	25.0	14.2
Mean downslope curvature (-)	+0.05	-0.08	-0.08

Assessment of thermal ground conditions indicates that the debris flow initiation site is subjected to a high energy environment. Potential incoming solar radiation reaches  $2,135 \text{ kWh m}^{-2} \text{ a}^{-1}$  (Fig. 5c). The Alpine Permafrost Index Map indicates that the initiation zone is located at the lower permafrost boundary, with permafrost preserved only in very favorable conditions (Fig. 5d). Collectively, the convex morphology and exposed position, strong potential radiation and unfavorable permafrost index are conducive to an advanced stage of permafrost degradation, increased water contents, and large amounts of unfrozen, loose sediment susceptible to mobilization (Marcer et al., 2019).

Grain size analyses indicate that the blocky surface layer of Hüttekarak Rock Glacier is composed of poorly sorted, coarse-grained sediment. The finer-grained parts, measured on three locations (1–3; positions given in Fig. 3), show an average grain size of 11.6, 12.8, and 16.0 cm, respectively. The coarse-grained site (4) exhibits an average grain size of 65.6 cm, documenting the heterogeneous structure of the blocky surface layer. Figure 6a displays the respective grain-size distributions. Due to the subordinate presence of components smaller than gravel (largely matrix-free surface layer), the rock glacier classifies as bouldery rock glacier sensu Ikeda and Matsuoka (2006). These characteristics indicate a permeable surface layer exhibiting high infiltration capacity and low hydraulic resistance to water flowing along the permafrost table.

Sieve analyses of samples 5–8 taken at the rock glacier front (Fig. 6b, positions indicated in Fig. 3) show that gravel (64 %) and sand (25 %) are the dominating grain sizes, while the amount of clay and silt is very low (< 1 %). The samples are extremely poorly sorted (4.4 after Folk and Ward (1957)). Loose deposits of sediments exhibiting similar grain size distributions are well known to respond to shearing in a contractive manner and constitute characteristic debris flow material (Iverson, 1997; Savage and Baum, 2005). Experimental investigations of similarly composed source material confirm these observations (dashed lines in Fig. 6b), identifying contractive response to shearing and pore pressure diffusion timescales exceeding the duration of debris flow motion as major prerequisites for mobilization (Major, 1996; Iverson, 1997). Provided sufficient water is available to keep the rock glacier debris saturated, these characteristics promote the development of undrained loading conditions, high sensitivity of effective stresses to sediment compaction and perpetually high excess pore-water pressures in response to deformation (Major, 1996; Iverson, 1997; Major et al., 1997). These features document the compositional propensity of the rock glacier front to debris flow mobilization.

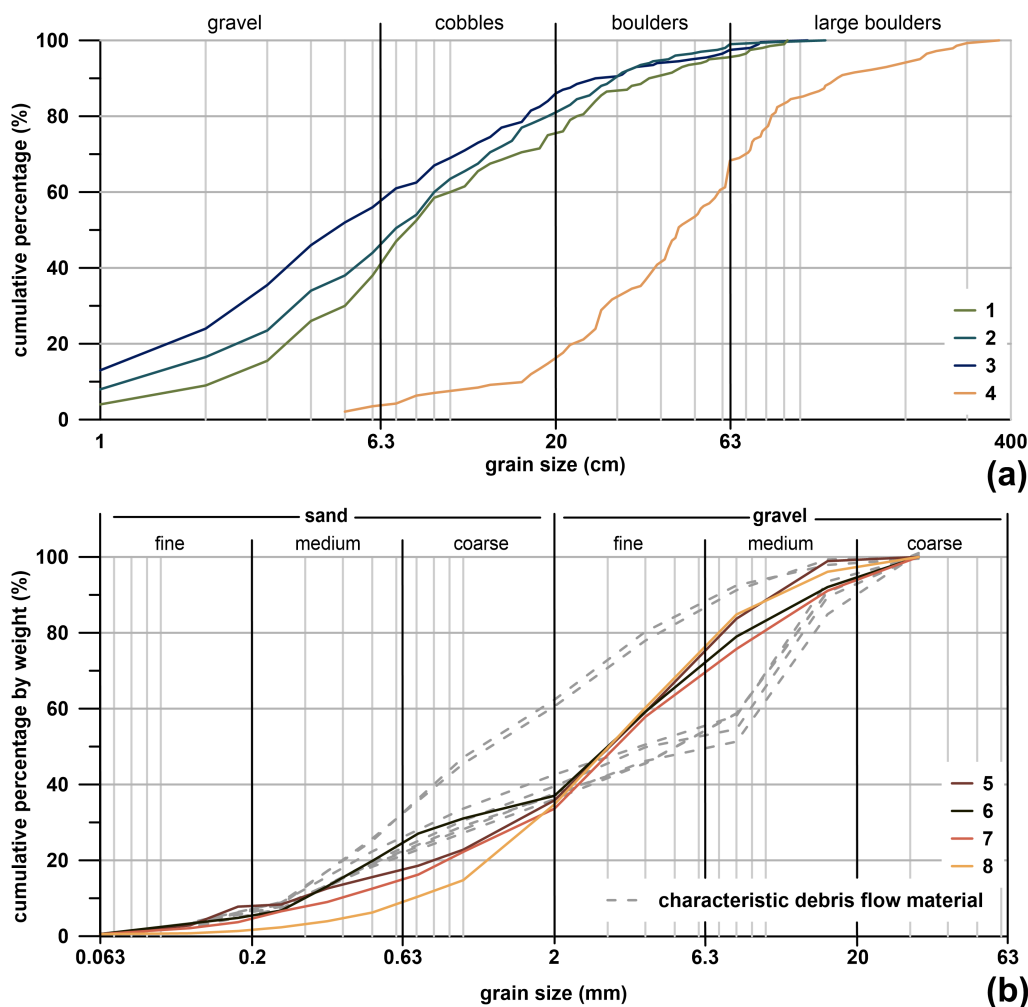


**Figure 6.** Grain-size distributions of Hüttekark Rock Glacier surface layer (a) and front material (b). The corresponding sampling locations are indicated in Fig. 3. Dashed grey lines represent source compositions of a set of experimentally investigated debris flows showing contractive shear response and undrained failure (USGS debris flow flume; Major (1996); Iverson (1997); Iverson et al. (1997)). Classification according to ISO 14688-1 (International Organization for Standardization, 2017).

## 5.2 Preparatory factors

Analysis of multi-temporal ortho-images indicates constant, moderate surface displacement rates. The kinematics of the rock glacier surface show mean annual surface displacement rates of the 200 prominent blocks ranging from 1–50 cm a<sup>-1</sup> (mean: 14 cm a<sup>-1</sup>) in the observation period of 1970–2020. The position of the rock glacier front fluctuates non-directionally (amplitude 3–7 m), indicating that steady erosion of the front approximately balances rock glacier movement, thus ensuring an invariant long-term front geometry (Kummert and Delaloye, 2018). While destabilization of rock glaciers is frequently characterized



**Table 3.** Climate analysis highlighting the warm and moderately dry conditions prevailing during summer 2019, preceding the debris flow. In addition, air temperature and positive degree day sum show a strong long-term trend, promoting permafrost degradation in Hüttekarkirque. Angle brackets indicate average values, insignificant trends (at the  $\alpha = 0.05$  level) are given in rounded brackets.

Parameter	Air temperature	Positive degree day sum	Precipitation	Precipitation due to very wet days
Summer 2019	7.0 °C	519 °C	329 mm	102 mm
Summer <1976–2019>	4.6 °C	358 °C	346 mm	97 mm
<2019>	-1.5 °C	842 °C	1,348 mm	359 mm
<1976–2019>	-2.5 °C	653 °C	1,042 mm	245 mm
Trend magnitude	+0.05 °C a <sup>-1</sup>	+7.2 °C a <sup>-1</sup>	(+0.13 mm a <sup>-1</sup> )	(+0.05 mm a <sup>-1</sup> )
Trend significance ( <i>p</i> -value)	2.4 × 10 <sup>-13</sup>	3.3 × 10 <sup>-7</sup>	(3.7 × 10 <sup>-1</sup> )	(9.9 × 10 <sup>-1</sup> )

by accelerating surface deformation rates and the development of surface discontinuities such as cracks and crevasses, the absence of these features on Hüttekarkirque does not point towards general destabilization of the rock glacier before the 2019 debris flow. However, after the debris flow, a cluster of collapse structures connecting the shallow depression hosting the thermokarst lake and the debris flow initiation zone is clearly recognizable (Fig. S2; Government of the Province of Tyrol (2021b)).

Analyzing the long-term (1976–2019) climate signal highlights the distinct hydrometeorological characteristics of the months preceding the failure and the respective long-term trends in Hüttekarkirque (Table 3). In 2019, the summer months show exceptionally high air temperatures compared to the long-term average (+2.4 °C). The high positive degree day sum (+161 °C) reflects the large amount of energy available for melting (Table 3). Total precipitation is moderately low (-17 mm) and slightly concentrated on very wet days (+5 mm) with respect to the long-term average (Table 3). The climate data record shows significantly increasing air temperature (+0.05 °C a<sup>-1</sup>, exceeding corresponding trends at the global and European Alps scale (+0.02 (±0.01) and +0.03 (±0.02) °C a<sup>-1</sup>, respectively; Hock et al. (2019))) and positive degree day sum (+7.2 °C a<sup>-1</sup>). In contrast, neither total precipitation nor precipitation due to very wet days increase significantly during the 43 years preceding the debris flow (at the  $\alpha = 0.05$  level). Recapitulating, the months preceding the debris flow are characterized by warm and dry conditions, on top of an exceptionally strong long-term trend of increasing air temperature in Hüttekarkirque.

Figure 7 depicts the inter-annual comparison of snowmelt, ice melt and rainfall (normalized to catchment area), indicating moderately wet conditions anteceding the debris flow. Intense snowmelt and ice melt (11.2 and 2.7 mm d<sup>-1</sup>, respectively) reflect the high energy available in 2019, in agreement with the high positive degree day sum reported above. The winter season preceding the debris flow is characterized by a prominent snow cover, almost monotonically gaining volume until 29 May 2019, roughly restricting meltwater production to June. The long-lasting snow cover and rapid snowmelt (Fig. 7b) is in excellent agreement with observations throughout Tyrol (Hydrological Service of Tyrol, 2019). Comparing total volumes indicates inconspicuous overall conditions in 2019 (Fig. 7c), acknowledging that the relatively short record precludes statistically substantiated conclusions.

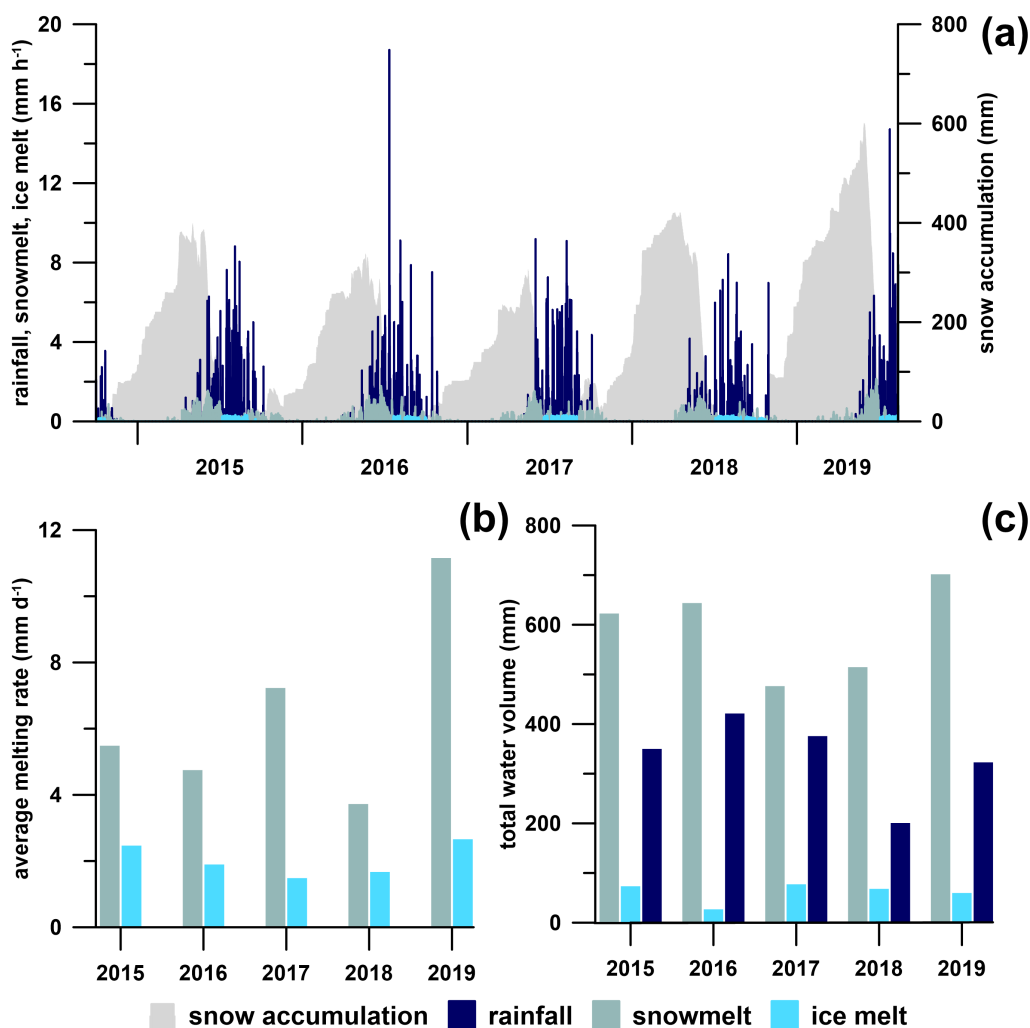


**Figure 7.** (a) Time series of rainfall, snowmelt and ice melt in Hüttekarak based on INCA (Haiden et al., 2011) and SNOWGRID (Olefs et al., 2013). The snow cover dynamics in spring 2019 differ from the preceding years by the late and rapid snowmelt. (b) Average snowmelt and ice melt rates for individual years (linear approximation). Spring 2019 is characterized by exceptionally high snowmelt rates. (c) Total water volumes (between 01 January and 13 August) per year, attributed to rainfall, snowmelt and ice melt, respectively. Despite the different snow cover dynamics in spring 2019, the total meltwater volume exceeds the respective volume of the preceding years only slightly.

### 5.3 Triggering factors

The rainfall event preceding the debris flow lasted for 74 h at an average intensity of 0.54 mm h<sup>-1</sup> (total rainfall volume ~40 mm). The frequency analysis shows that 12 % of earlier rainfall events hitting Hüttekarak-cirque exceeded it in severity (Fig. 8). The event does not exceed the regional critical rainfall thresholds for debris flow initiation during the summer season with

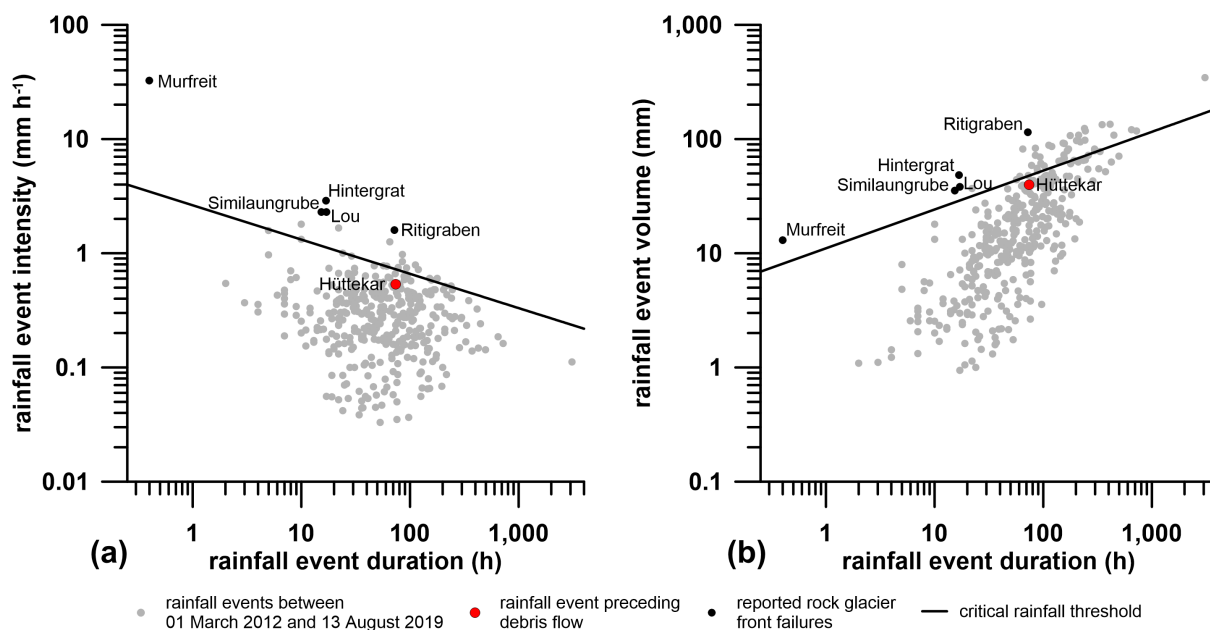


**Figure 8.** Rainfall event frequency analysis with respect to (a) rainfall intensity-duration and (b) rainfall volume-duration based on INCA (Haiden et al., 2011). The rainfall event preceding the Hüttekär debris flow (red dot) was neither especially intense nor especially persistent with respect to earlier rainfall events hitting Hüttekär-cirque (grey dots), critical rainfall thresholds (black lines) and rainfall events triggering documented rock glacier front failures in the European Alps (black dots) (note logarithmic scale). Regional thresholds describing minimum conditions for rainfall-induced debris flows are based on Nikolopoulos et al. (2015b) and Marra et al. (2016). Characteristics of documented triggering events are based on Lugon and Stoffel (2010); Krainer et al. (2012); Kofler et al. (2021); Marcer et al. (2020).

335 respect to intensity-duration (Fig. 8a; Nikolopoulos et al. (2015b)) and volume-duration (Fig. 8b; Marra et al. (2016)), although  
 these are regarded conservative estimates (Wieczorek and Guzzetti, 2000; Guzzetti et al., 2007). These characteristics distinctly  
 contrast with the rainfall events preceding well documented rock glacier front failures in the European Alps that occurred in  
 response to heavy rainfall (Fig. 8): the Ritigraben event on 24 September 1993 (Lugon and Stoffel, 2010), the Murfreit event  
 on 02 July 2003 (Krainer et al., 2012), the Hintergrat and Similaungrube events, both on 13 August 2014 (Kofler et al., 2021),  
 340 as well as the Lou event on 14 August 2015 (Marcer et al., 2020).

Field observations as well as satellite data analysis detect the rapid evolution and drainage of the thermokarst lake that  
 was formed on the rock glacier surface. Sentinel-2 satellite imagery indicates water pooling in the depression on 03 June  
 2019, when snow still covered large parts of the rock glacier catchment (520 mm average snow water equivalent based on  
 SNOWGRID). The thermokarst lake evolved over a period of 10 weeks, but drained within hours through a newly formed  
 345 channel, indicating that the characteristic time scale of thermokarst breakthrough is shorter than the summer season (Fig. 4e-h,  
 Fig. S2). Comparing snow cover and lake development shows that the latter gained most of its volume during the intense  
 snowmelt period in June (Fig. 8a). Linear interpolation of the lake surface area between the cloud-free satellite imagery dates



**Table 4.** Thermokarst lake development based on INCA (Haiden et al., 2011), Sentinel-2 satellite data (Sentinel Hub, 2020) and the most recent (2017) high-resolution DTM of the rock glacier surface (Government of the Province of Tyrol, 2021a).

Date	Surface area (m <sup>2</sup> )	Water volume (m <sup>3</sup> ) <sup>a</sup>	Mean water depth (m)	Total energy input (J) <sup>b</sup>	Total ice melt (m <sup>3</sup> ) <sup>b</sup>
01 June 2019	0	0	0	0	0
03 June 2019	1,520	1,320	0.9	$2.9 \times 10^{10}$	100
13 June 2019	21,370	68,340	3.2	$1.6 \times 10^{12}$	5,410
16 June 2019	26,380	97,020	3.7	$2.7 \times 10^{12}$	8,850
18 June 2019	28,570	110,760	3.9	$3.4 \times 10^{12}$	11,180
26 June 2019	31,670	131,870	4.2	$6.3 \times 10^{12}$	20,940
28 June 2019	34,010	148,290	4.4	$7.3 \times 10^{12}$	24,220
01 July 2019	35,650	158,770	4.5	$8.8 \times 10^{12}$	29,380
06 July 2019	36,400	162,370	4.5	$1.1 \times 10^{13}$	36,280
16 July 2019	36,960	166,040	4.5	$1.4 \times 10^{13}$	47,050
23 July 2019	36,960	166,040	4.5	$1.7 \times 10^{13}$	57,550
26 July 2019	36,960	166,040	4.5	$1.9 \times 10^{13}$	63,090
13 August 2019	36,960	166,040	4.5	$2.6 \times 10^{13}$	87,480

<sup>a</sup>estimate based on DTM (2017) <sup>b</sup>since 01 June 2019

enables the calculation of the total energy input to the lake (Table 4). While the area gain slowed down at the beginning of July, the energy input was considerable thereafter, allowing for extensive ice melt beneath the surface. The total amount of ice melt preceding the failure sums to  $\sim 87,000 \text{ m}^3$  (corresponding energy input  $2.6 \times 10^{13} \text{ J}$ ). The impact of energy available for thermokarst evolution is emphasized by dividing this value by the distance to the debris flow initiation zone ( $\sim 350 \text{ m}$ ), and assuming a channel of circular cross section, resulting in an upper bound estimate of 18 m for the channel diameter. While only a fraction of this energy is actually involved in channel development, the resulting order of magnitude clearly demonstrates the potential of thermokarst evolution for triggering the lake outburst during the course of a single summer season. Dividing the latest lake water volume estimate ( $\sim 166,000 \text{ m}^3$ ) by the drainage time ( $\sim 1 \text{ day}$ ) indicates a drainage rate on the order of  $\sim \text{m}^3 \text{ s}^{-1}$ , supplying a substantial amount of water to the debris flow initiation zone. In contrast to many hazardous glacial lakes evolving over time scales of years to decades (Haerberli, 1983; Mölg et al., 2021), the thermokarst lake in Hüttekarcirque unfolded its destructive power already two months after its formation.

## 6 Discussion

While the absence of instrumentation in Hüttekarcirque during the failure inhibits a detailed reconstruction of the debris flow initiation mechanism, the relative importance of destabilizing factors can confidently be evaluated.



Unfavorable topographical and sedimentological predisposition put the rock glacier front in a state susceptible to debris flow initiation. Its steep slope angle supports shear stress and sensitivity to liquefaction while lowering shear strength (Iverson et al., 1997; Chowdhury et al., 2010; Reichenbach et al., 2018). Convex topography generally induces extensive deformation patterns favoring the development of tensional stresses (Roer et al., 2008; Delaloye et al., 2013; Marcer et al., 2019). Since the rock glacier did not show discernible signs of destabilization prior to debris flow initiation, external drivers including the strong increase in air temperature and positive degree day sum, along with available snow and ice meltwater and their pronounced impact on permafrost during the months preceding the debris flow event are considered crucial preparatory factors (Table 3). Rock glacier creep balancing erosion rates in combination with a high energy environment favoring permafrost degradation at the rock glacier front provide a large accumulation of loose, unfrozen sediment that is susceptible to mobilization down the adjacent steep slope (Fig. 5, Fig. S2).

Debris slides within saturated, loose sediment responding contractive to shear deformation are prone to mobilize into debris flows (Savage and Baum, 2005). Collapse of the soil structure and crushing of particles drives the development of transient excess pore-water pressures in parts of the deforming mass, which reacts by disintegration and acceleration (Hutchinson and Bhandari, 1971; Iverson and Major, 1986; Anderson and Sitar, 1995; Iverson, 1997, 2005, 1997; Sassa and Wang, 2005). Within the displaced mass, the rates of excess pore-water pressure generation and dissipation critically depend on strain rate, bulk density, and grain size distribution (Iverson, 1997, 2005; Iverson et al., 1997). Poorly sorted sand and gravel, such as the Hüttekark Rock Glacier material (Fig. 6b), are susceptible to undrained deformation and attendant pore-water pressure coevolution, demonstrating the susceptibility of the rock glacier to debris flow mobilization (Iverson, 1997, 2005; Iverson et al., 1997). The relative time scales for pore space contraction and pore-water pressure diffusion govern the persistence of high pore-water pressures (Iverson, 1997; Iverson and LaHusen, 1989; Iverson et al., 1997). The diffusion time scale of Hüttekark Rock Glacier debris is relatively short (on the order of  $\sim 20$  s, estimated from similar material investigated at the USGS debris flow flume, Fig. 6b; Iverson (1997)). Sustaining pore-water pressures high enough to keep debris flow surges in motion therefore requires rapid and persistent delivery of large amounts of water (on the order of a few  $\text{m}^3 \text{s}^{-1}$ ).

Frequency analysis of rainfall events hitting Hüttekark-cirque indicates that the event immediately preceding the debris flow was not exceptionally severe, falling below the critical threshold for failure initiation (Fig. 8). Regarding the moderately dry hydrometeorological conditions during summer 2019 (Table 3), these observations suggest that the storm immediately preceding the event fails to provide the large amounts of water necessary to initiate and sustain the debris flow for several hours. Considering the coincident thermokarst lake outburst, following exceptionally warm weeks characterized by considerable energy input promoting melting processes and permafrost degradation (Table 3, Table 4), a multiple trigger mechanism is regarded plausible instead.

The key issue in terms of debris flow mechanics is the rate of water transport to the initiation zone. Field evidence suggests that water flowed concentrated along a newly formed channel network from the thermokarst lake to the rock glacier front (Fig. 4e, Fig. 4f, Fig. 4h, Fig. S2). The rapid development of this efficient drainage network was facilitated by the short timescale of advective heat transport along the meltwater channels. Driven by thermal convection, the establishment of such a channel system was possible within several weeks, despite the considerable distance of  $\sim 350$  m. The energy provided by the



thermokarst lake strikingly exceeded the latent heat of fusion necessary for channel evolution. Once established, this channel network provided the capability to transport large amounts of water from the thermokarst lake to the debris flow initiation zone within a short time. Water flow velocities along these highly permeable flow paths may reach up to several  $\text{cm s}^{-1}$  (Tenthorey, 1992; Krainer and Mostler, 2002; Buchli et al., 2013; Wagner et al., 2021b), providing sufficient water to the debris flow to keep the deforming sediment saturated. Consequently, rapid drainage emptied the lake within hours, without apparent prior indications of a lake outburst.

With respect to GLOF hazard evaluation, the decisive factor is that thermokarst development and breakthrough happened within an extremely short time scale (on the order of weeks), driven by the high energy input during summer 2019. In terms of mechanical properties, the ice-debris mixture composing the rock glacier represents a transitional form between the common glacier dammed and moraine dammed lakes (Clague and Evans, 1994; Huggel et al., 2004; Schaub, 2015). The Hüttekarak Rock Glacier failure mechanism involved drainage channel enlargement as well as collapse of the rock glacier front, demonstrating that thermokarst development and slope failure operated synergistically. Since their contrasting time scales ( $\sim$ weeks for channel enlargement,  $\sim$ seconds to hours for rock glacier front collapse) are commonly associated with different materials (ice and debris, respectively), the integration of both mechanisms distinguishes rock glaciers from glaciers and moraines in terms of GLOF hazard assessment. The large amounts of debris provided by the rock glacier favored the evolution of the outburst flood into a debris flow.

Subsequently, the hazard cascade triggered in Hüttekarak-cirque was expanded by an additional element when the displaced mass reached and blocked Radurschlbach, impounding a voluminous ( $\sim 120,000 \text{ m}^3$ ) lake that threatened a large area downstream. Acknowledging that landslide dams frequently fail within a short period (hours to months) after their formation, and that common failure mechanisms including overtopping, piping and mechanical collapse are capable of triggering severe outburst floods, prediction and instant detection of these events in remote areas is crucial for risk assessment in mountainous areas (Clague and Evans, 1994; Ermini and Casagli, 2003; Schaub, 2015).

## 7 Conclusions

The 2019 Hüttekarak debris flow impounded the main river of Radurschl Valley, threatening the downstream community and infrastructure by dam breakthrough. The rock glacier front failure was caused by an upstream thermokarst lake outburst and mobilized into a catastrophic debris flow displacing  $40,000\text{--}50,000 \text{ m}^3$  within several hours. Analyzing a comprehensive set of potentially destabilizing factors reveals critical combinations of environmental influences that govern multi hazard characteristics in a complex periglacial setting. Evaluating the topographical and sedimentological context, quantifying rock glacier movement rates preceding the failure, and analyzing climate and weather signals demonstrates the capability of rapid thermokarst evolution to induce highly hazardous situations at short time scales. In combination with challenges regarding hazard detection and prediction in remote areas, this complicates integrated multi hazard assessment (Kappes et al., 2012; Gallina et al., 2016). In this context, the combination of several raster data sets comprising terrain models, satellite imagery, and gridded climate and



weather variables proofed a valuable tool for assessing the individual impact of destabilizing factors in complex mountainous  
430 terrain.

The observed failure differs from rock glacier front failures documented so far. Not only the amount of rainfall, but its  
combination with the thermokarst lake development, and the evolution of a drainage system within the rock glacier caused the  
debris flow. The fact that a comparable thermokarst lake had never been observed before on Hüttekark Rock Glacier, and that the  
outburst occurred only two months after its formation imply that comparable lake formation and outburst are hardly predictable.  
435 As climate change progresses, this mechanism will likely gain importance due to accelerated permafrost degradation and  
increased energy available for thawing, altering ground properties and increasing the likelihood of thermokarst lake formation  
(Kääb and Haeberli, 2001; Patton et al., 2019). Since many rock glacier fronts exhibit grain size distributions similar to the  
Hüttekark Rock Glacier (Johnson, 1992; Haeberli and Vonder Mühll, 1996; Arenson et al., 2002; Krainer et al., 2010, 2012),  
they pose widespread multi hazard elements in mountainous regions, with significantly increased risk if rivers or infrastructure  
440 pass potential runout zones of debris flows.

The observed debris flow mechanism is the most frequent one in colluvium, which covers most of the surface in mountain-  
ous terrain (Turner, 1996). Thus, we suggest that the results obtained in this study apply not only to rock glaciers, but to a  
wide range of colluvium in mountainous, permafrost-affected landscapes, with accordingly wide implications. Including rapid  
thermokarst evolution in landslide hazard assessment gains importance as climate change progresses, altering the boundary  
445 conditions for periglacial landslides across the European Alps and mountain ranges around the world. The developed process-  
based understanding of the analyzed hazard cascade including thermokarst lake outburst, rock glacier front failure, debris flow  
evolution, and river blockage provides an expedient tool for multi hazard identification.

*Data availability.* Input data for this study are freely available. Meteorological data sets (SPARTACUS, INCA) are provided by the Central  
Institute for Meteorology and Geodynamics (<https://data.hub.zamg.ac.at/>, last access: 28 June 2022). The Government of the Province of  
450 Tyrol provides the digital terrain model as well as current and historical ortho-images (<https://www.data.gv.at/>, last access: 28 June 2022).  
Sentinel-2 multi-spectral satellite data are provided by Copernicus and processed by Sentinel Hub (<https://www.sentinel-hub.com/>, last  
access: 28 June 2022).

## Appendix A

Ice ablation rates  $m$ , given as ice water equivalent ( $\text{m s}^{-1}$ ), are calculated using a surface energy balance approach (Cuffey and  
455 Paterson, 2010):

$$m = \frac{Q_r + Q_h + Q_e + Q_p}{\lambda_f \rho_w} \quad (\text{A1})$$

where  $Q_r$  is net radiation ( $\text{W m}^{-2}$ ),  $Q_h$  is the sensible heat flux ( $\text{W m}^{-2}$ ),  $Q_e$  is the latent heat flux ( $\text{W m}^{-2}$ ),  $Q_p$  is the heat  
flux associated with precipitation ( $\text{W m}^{-2}$ ),  $\lambda_f$  is the latent heat of fusion ( $3.34 \times 10^5 \text{ J kg}^{-1}$ ), and  $\rho_w$  is the density of water ( $\text{kg}$



m<sup>-3</sup>) at 273.15 K. Equation (A1) assumes the glacier surface to stay at 273.15 K and neglects transfer of heat within the glacier,  
460 both assumptions considered reasonable approximations for the ablation zones of temperate glaciers during the summer season  
(Hock, 2005; Cuffey and Paterson, 2010). For the operational purposes of this study, estimates of the individual energy flux  
contributions aim at evaluating their variation between different years rather than yielding precise absolute values. Net radiation  
is calculated according to (Cuffey and Paterson, 2010):

$$Q_r = Q_s(1 - \alpha) + \epsilon_a \sigma T_a^4 - \epsilon_s \sigma T_s^4 \quad (\text{A2})$$

465 where  $Q_s$  is incoming shortwave radiation (W m<sup>-2</sup>),  $T_a$  is air temperature (K),  $T_s$  is surface temperature (K),  $\alpha$  is broadband  
surface albedo (-),  $\epsilon_a$  is atmospheric emissivity (-),  $\epsilon_s$  is surface emissivity (-), and  $\sigma$  is the Stefan-Boltzmann constant (5.67  
 $\times 10^{-8}$  W m<sup>-2</sup> K<sup>-4</sup>). As a first approximation,  $\epsilon_s \approx 0.95$  for ice and water, while  $\alpha \approx 0.4$  and  $\alpha \approx 0.06$  for ice and water,  
respectively (Cuffey and Paterson, 2010). Incoming shortwave radiation is given by the superposition of direct and diffuse  
radiation, accounting for cloudiness (INCA) and the shadowing effect of surrounding terrain, as well as by shortwave radiation  
470 reflected by the surrounding terrain ( $\alpha \approx 0.2$ , GRASS GIS 8.0, Hofierka et al. (2007)). Atmospheric emissivity is parameterized  
as outlined by Greuell et al. (1997) and Oerlemans (2000). Sensible and latent heat fluxes are calculated by parameterization  
of the respective transport processes based on turbulence similarity assuming a roughness length of 10<sup>-2</sup> m (Brutsaert, 2005;  
Brock et al., 2006; Cuffey and Paterson, 2010). The sensible heat flux is given by:

$$Q_h = c_a \rho_a C_h u (T_a - T_s) \quad (\text{A3})$$

475 where  $c_a$  is the specific heat capacity of air at constant pressure (1006 J kg<sup>-1</sup> K<sup>-1</sup>),  $C_h$  is the heat transfer coefficient (Stanton  
number) (-),  $u$  is windspeed (m s<sup>-1</sup>), and  $\rho_a$  is air density (kg m<sup>-3</sup>). The latent heat flux is obtained using:

$$Q_e = \lambda_v \rho_a C_e u (x_a - x_s) \quad (\text{A4})$$

where  $C_e$  is the water vapor transfer coefficient (Dalton number) (-),  $x_a$  is the specific humidity of air (-),  $x_s$  is the specific  
humidity at the surface (-), and  $\lambda_v$  is the latent heat of vaporization (2.5  $\times 10^6$  J kg<sup>-1</sup>). The heatflux associated with precipitation  
480 is estimated assuming that the rain droplet temperature  $T_d$  approaches the near-surface air temperature:

$$Q_p = c_w \rho_w P (T_d - T_s) \quad (\text{A5})$$

where  $c_w$  is the specific heat capacity of water at constant pressure (4219 J kg<sup>-1</sup> K<sup>-1</sup>), and  $P$  is the precipitation intensity (m  
s<sup>-1</sup>).

The plausibility of the calculated ablation rates is evaluated by comparing them to a set of glacier ablation rates and associated  
485 energy flux contributions across the European Alps (Table A1). The results obtained for Hüttekarferner and Glockturmferner



(Table A2) fall within the range given by this sample, reflecting the northward exposition and steep slope of both glaciers by comparatively smaller total ablation rates.

**Table A1.** Ablation rates and energy flux contributions measured and calculated at various glaciers across the European Alps (Escher-Vetter, 1985; Greuell and Oerlemans, 1989; van de Wal et al., 1992; Greuell et al., 1997; Arnold et al., 1996; Oerlemans, 2000; Brock et al., 2000; Klok and Oerlemans, 2002; Oerlemans and Klok, 2002; Willis et al., 2002; Brock et al., 2006; Oerlemans et al., 2009). Values represent averages taken over the outlined period (altitude Alt (m a.s.l.), slope Sl (°), aspect Asp, measured ice ablation rate  $m$  (cm day<sup>-1</sup>), given as water equivalent assuming an ice density of 900 kg m<sup>-3</sup>, total energy flux density  $Q$  (W m<sup>-2</sup>), net shortwave radiation  $Q_s$  (W m<sup>-2</sup>), net longwave radiation  $Q_l$  (W m<sup>-2</sup>), sensible heat flux  $Q_h$  (W m<sup>-2</sup>), and latent heat flux  $Q_e$  (W m<sup>-2</sup>), Austria AT, Switzerland CH). The (small) precipitation heat flux is rarely reported, thus not included.

Location	Alt	Sl	Asp	Period	$m$	$Q$	$Q_s$	$Q_l$	$Q_h$	$Q_e$
Haut Glacier d'Arolla (Pennine Alps, CH)	2,964	16	N	30 May 1990–28 August 1990	3.8	101	130	-52	26	-3
Haut Glacier d'Arolla (Pennine Alps, CH)	2,964	16	N	10 August 1993–25 August 1993	6.9	167	165	-20	10	12
Hintereisferner (Ötztal Alps, AT)	3,037	16	NE	12 July 1986–22 July 1986	5.1	210	236	-45	22	-3
Hintereisferner (Ötztal Alps, AT)	3,037	16	NE	13 July 1989–30 July 1989	7.9	158	155	-8	32	-21
Pasterze <sup>a</sup> (Glockner Range, AT)	2,914	16	E	18 June 1994–7 August 1994	5.9	232	194	-16	45	9
Pasterze <sup>b</sup> (Glockner Range, AT)	2,914	16	E	21 June 1994–12 August 1994	6.3	236	185	-17	56	12
Pasterze <sup>c</sup> (Glockner Range, AT)	2,914	16	E	19 June 1994–12 August 1994	6.5	242	199	-19	53	9
Pasterze <sup>d</sup> (Glockner Range, AT)	2,914	16	E	15 June 1994–16 August 1994	3.0	109	119	-33	20	3
Pasterze <sup>e</sup> (Glockner Range, AT)	2,914	16	E	15 June 1994–16 August 1994	2.0	87	109	-39	19	-2
Vadret da Morteratsch (Bernina Range, CH)	3,079	21	N	01 October 1995–30 September 1998	1.6	191	177	-25	31	8
Vadret da Morteratsch (Bernina Range, CH)	3,079	21	N	01 June 1999–31 August 1999	4.0	171	139	-17	37	12
Vadret da Morteratsch (Bernina Range, CH)	3,079	21	N	01 June 2000–31 August 2000	4.7	166	140	-27	43	10
Vadret da Morteratsch (Bernina Range, CH)	3,079	21	N	01 June 2001–31 August 2001	4.8	179	147	-29	49	12
Vadret da Morteratsch (Bernina Range, CH)	3,079	21	N	01 June 2002–31 August 2002	4.9	185	144	-22	48	15
Vadret da Morteratsch (Bernina Range, CH)	3,079	21	N	01 June 2003–31 August 2003	5.7	240	173	-24	70	21
Vadret da Morteratsch (Bernina Range, CH)	3,079	21	N	01 June 2004–31 August 2004	4.7	189	158	-24	42	13
Vadret da Morteratsch (Bernina Range, CH)	3,079	21	N	01 June 2005–31 August 2005	4.9	203	173	-23	42	11
Vadret da Morteratsch (Bernina Range, CH)	3,079	21	N	01 June 2006–31 August 2006	5.5	215	181	-23	50	7
Vernagtferner (Ötztal Alps, AT)	3,166	14	S	01 June 1982–30 September 1982	1.4	57	82	-24	38	-39

<sup>a</sup>weather station at 2205 m a. s. l. <sup>b</sup>weather station at 2310 m a. s. l. <sup>c</sup>weather station at 2420 m a. s. l. <sup>d</sup>weather station at 2945 m a. s. l. <sup>e</sup>weather station at 3225 m a. s. l.

*Author contributions.* SK, TW, KK, and GW designed the study and prepared the initial draft. Formal analysis, methodology development, data collection, and visualization were performed by SK, TW, KK, MA and MO. MA, MO and KH edited and complemented the manuscript draft. GW managed and coordinated the project, including the funding acquisition.



**Table A2.** Ablation rates and energy flux contributions calculated in this study. Values represent averages taken over the outlined period (altitude Alt (m a.s.l.), slope Sl ( $^{\circ}$ ), aspect Asp, measured ice ablation rate  $m$  ( $\text{cm day}^{-1}$ ), given as water equivalent assuming an ice density of  $900 \text{ kg m}^{-3}$ , total energy flux density  $Q$  ( $\text{W m}^{-2}$ ), net shortwave radiation  $Q_s$  ( $\text{W m}^{-2}$ ), net longwave radiation  $Q_l$  ( $\text{W m}^{-2}$ ), sensible heat flux  $Q_h$  ( $\text{W m}^{-2}$ ), and latent heat flux  $Q_e$  ( $\text{W m}^{-2}$ )).

Location	Alt	Sl	Asp	Period	$m$	$Q$	$Q_s$	$Q_l$	$Q_h$	$Q_e$
Glockturmferner	2,855	27	N	01 June 2015–31 August 2015	2.5	90	84	-14	28	-8
Glockturmferner	2,855	27	N	01 June 2016–31 August 2016	2.2	77	77	-17	19	-2
Glockturmferner	2,855	27	N	01 June 2017–31 August 2017	2.5	91	78	-11	31	-7
Glockturmferner	2,855	27	N	01 June 2018–31 August 2018	2.2	79	79	-16	21	-5
Glockturmferner	2,855	27	N	01 June 2019–31 August 2019	2.6	97	82	-12	30	-3
Hüttekarferner	3,043	21	N	01 June 2015–31 August 2015	3.9	145	135	-9	32	-13
Hüttekarferner	3,043	21	N	01 June 2016–31 August 2016	3.5	127	123	-12	24	-8
Hüttekarferner	3,043	21	N	01 June 2017–31 August 2017	3.7	139	125	-6	32	-12
Hüttekarferner	3,043	21	N	01 June 2018–31 August 2018	3.6	133	127	-10	26	-10
Hüttekarferner	3,043	21	N	01 June 2019–31 August 2019	3.9	146	134	-8	27	-7

*Competing interests.* The authors declare that they have no conflict of interest.

*Acknowledgements.* This research was funded by the Austrian Federal Ministry of Agriculture, Regions and Tourism and the Federal Provinces of Vorarlberg, Tyrol, Salzburg, Styria and Carinthia within the DaFNE project RG-AlpCatch. We thank Josef Waldner and Gerhard Schaffenrath for witness reports, local information, discussion, and photographs. Additional photographs and information were kindly provided by Roman Außerlechner, Thomas Figl, Werner Thöny (Geological Survey of Tyrol), Rudolf Philippitsch, Danny F. Minahan, Ainur Kokimova, and Irène Apra. The authors acknowledge the financial support by the University of Graz.

495



## References

- Adler, C., Wester, P., Bhatt, I., Huggel, C., Insarov, G. E., Morecroft, M. D., Muccione, V., and Prakash, A.: Cross-Chapter Paper 5: Mountains, in: *Climate Change 2022: Impacts, Adaptation, and Vulnerability*, edited by Intergovernmental Panel on Climate Change, Cambridge University Press, 2022.
- Anderson, R. S., Anderson, L. S., Armstrong, W. H., Rossi, M. W., and Crump, S. E.: Glaciation of alpine valleys: The glacier – debris-covered glacier – rock glacier continuum, *Geomorphology*, 311, 127–142, <https://doi.org/10.1016/j.geomorph.2018.03.015>, 2018.
- Anderson, S. A. and Sitar, N.: Analysis of Rainfall-Induced Debris Flows, *Journal of Geotechnical Engineering*, 121, 544–552, [https://doi.org/10.1061/\(ASCE\)0733-9410\(1995\)121:7\(544\)](https://doi.org/10.1061/(ASCE)0733-9410(1995)121:7(544)), 1995.
- 500 Arenson, L., Hoelzle, M., and Springman, S.: Borehole deformation measurements and internal structure of some rock glaciers in Switzerland, *Permafrost and Periglacial Processes*, 13, 117–135, <https://doi.org/10.1002/ppp.414>, 2002.
- Arenson, L. U. and Springman, S. M.: Mathematical descriptions for the behaviour of ice-rich frozen soils at temperatures close to 0 °C, *Canadian Geotechnical Journal*, 42, 431–442, <https://doi.org/10.1139/T04-109>, 2005.
- Arenson, L. U., Hauck, C., Hilbich, C., Seward, L., Yamato, Y., and Springman, S.: Sub-surface Heterogeneities in the Murtèl – Corvatsch
- 510 Rock Glacier, Switzerland, in: *Proceedings of the joint 63rd Canadian Geotechnical Conference and the 6th Canadian Permafrost Conference*, edited by Canadian Geotechnical Society, pp. 1494–1500, Calgary, Alberta, 2010.
- Arnold, N. S., Willis, I. C., Sharp, M. J., Richards, K. S., and Lawson, W. J.: A distributed surface energy-balance model for a small valley glacier. I. Development and testing for Haut Glacier d’ Arolla, Valais, Switzerland, *Journal of Glaciology*, 42, 77–89, <https://doi.org/10.3189/S0022143000030549>, 1996.
- 515 Avian, M., Kaufmann, V., and Lieb, G. K.: Recent and Holocene dynamics of a rock glacier system: The example of Langtalkar (Central Alps, Austria), *Norsk Geografisk Tidsskrift - Norwegian Journal of Geography*, 59, 149–156, <https://doi.org/10.1080/00291950510020637>, 2007.
- Avian, M., Kellerer-Pirklbauer, A., and Bauer, A.: LiDAR for monitoring mass movements in permafrost environments at the cirque Hinteres Langtal, Austria, between 2000 and 2008, *Natural Hazards and Earth System Sciences*, 9, 1087–1094, [https://doi.org/10.5194/nhess-9-](https://doi.org/10.5194/nhess-9-1087-2009)
- 520 1087-2009, 2009.
- Beniston, M., Farinotti, D., Stoffel, M., Andreassen, L. M., Coppola, E., Eckert, N., Fantini, A., Giacomoni, F., Hauck, C., Huss, M., Huwald, H., Lehning, M., López-Moreno, J.-I., Magnusson, J., Marty, C., Morán-Tejeda, E., Morin, S., Naaim, M., Provenzale, A., Rabatel, A., Six, D., Stötter, J., Strasser, U., Terzago, S., and Vincent, C.: The European mountain cryosphere: A review of its current state, trends, and future challenges, *The Cryosphere*, 12, 759–794, <https://doi.org/10.5194/tc-12-759-2018>, 2018.
- 525 Bodin, X., Krysiecki, J.-M., Schoeneich, P., Le Roux, O., Lorier, L., Echelard, T., Peyron, M., and Walpersdorf, A.: The 2006 Collapse of the Bérard Rock Glacier (Southern French Alps), *Permafrost and Periglacial Processes*, 28, 209–223, <https://doi.org/10.1002/ppp.1887>, 2017.
- Boeckli, L., Brenning, A., Gruber, A., and Noetzi, J.: Alpine permafrost index map, <https://doi.org/10.1594/PANGAEA.784450>, supplement to: Boeckli, L et al. (2012): Permafrost distribution in the European Alps: calculation and evaluation of an index map and summary statistics. *The Cryosphere*, 6, 807–820, <https://doi.org/10.5194/tc-6-807-2012>, 2012a.
- 530 Boeckli, L., Brenning, A., Gruber, S., and Noetzi, J.: Permafrost distribution in the European Alps: Calculation and evaluation of an index map and summary statistics, *The Cryosphere*, 6, 807–820, <https://doi.org/10.5194/tc-6-807-2012>, 2012b.



- Borga, M., Stoffel, M., Marchi, L., Marra, F., and Jakob, M.: Hydrogeomorphic response to extreme rainfall in headwater systems: Flash floods and debris flows, *Journal of Hydrology*, 518, 194–205, <https://doi.org/10.1016/j.jhydrol.2014.05.022>, 2014.
- 535 Bracken, L. J., Turnbull, L., Wainwright, J., and Bogaart, P.: Sediment connectivity: A framework for understanding sediment transfer at multiple scales, *Earth Surface Processes and Landforms*, 40, 177–188, <https://doi.org/10.1002/esp.3635>, 2015.
- Brock, B. W., Willis, I. C., Sharp, M. J., and Arnold, N. S.: Modelling seasonal and spatial variations in the surface energy balance of Haut Glacier d’Arolla, Switzerland, *Annals of Glaciology*, 31, 53–62, <https://doi.org/10.3189/172756400781820183>, 2000.
- Brock, B. W., Willis, I. C., and Sharp, M. J.: Measurement and parameterization of aerodynamic roughness length variations at Haut Glacier  
540 d’Arolla, Switzerland, *Journal of Glaciology*, 52, 281–297, <https://doi.org/10.3189/172756506781828746>, 2006.
- Bronaugh, D.: PCIC Implementation of Climdex Routines: R package ‘climdex.pcic’, <https://cran.r-project.org/web/packages/climdex.pcic/>, last accessed 28 June 2022, 2020.
- Brunetti, M. T., Peruccacci, S., Rossi, M., Luciani, S., Valigi, D., and Guzzetti, F.: Rainfall thresholds for the possible occurrence of landslides in Italy, *Natural Hazards and Earth System Sciences*, 10, 447–458, <https://doi.org/10.5194/nhess-10-447-2010>, 2010.
- 545 Brutsaert, W.: *Hydrology: An Introduction*, Cambridge University Press, Cambridge, 2005.
- Buchli, T., Merz, K., Zhou, X., Kinzelbach, W., and Springman, S. M.: Characterization and Monitoring of the Furggwanghorn Rock Glacier, Turtmann Valley, Switzerland: Results from 2010 to 2012, *Vadose Zone Journal*, 12, <https://doi.org/10.2136/vzj2012.0067>, 2013.
- Buchli, T., Kos, A., Limpach, P., Merz, K., Zhou, X., and Springman, S. M.: Kinematic investigations on the Furggwanghorn Rock Glacier, Switzerland, *Permafrost and Periglacial Processes*, 29, 3–20, <https://doi.org/10.1002/ppp.1968>, 2018.
- 550 Buckel, J., Otto, J. C., Prasicek, G., and Keuschnig, M.: Glacial lakes in Austria - Distribution and formation since the Little Ice Age, *Global and Planetary Change*, 164, 39–51, <https://doi.org/10.1016/j.gloplacha.2018.03.003>, 2018.
- Burger, K. C., Degenhardt, J. J., and Giardino, J. R.: Engineering geomorphology of rock glaciers, *Geomorphology*, 31, 93–132, [https://doi.org/10.1016/S0169-555X\(99\)00074-4](https://doi.org/10.1016/S0169-555X(99)00074-4), 1999.
- Chowdhury, R., Bhattacharya, G., and Flentje, P.: *Geotechnical slope analysis*, CRC Press, Boca Raton, 2010.
- 555 Cicoira, A., Beutel, J., Faillettaz, J., and Vieli, A.: Water controls the seasonal rhythm of rock glacier flow, *Earth and Planetary Science Letters*, 528, 115 844, <https://doi.org/10.1016/j.epsl.2019.115844>, 2019.
- Clague, J. J. and Evans, S. G.: *Formation and failure of natural dams in the Canadian Cordillera*, 1994.
- Clague, J. J. and O’Connor, J. E.: Glacier-Related Outburst Floods, in: *Snow and Ice-Related Hazards, Risks, and Disasters*, edited by Haeberli, W., Whiteman, C., and Shroder, Jr., J. F., pp. 487–519, Elsevier, Amsterdam, 2015.
- 560 Clarke, G. K. C.: Glacier Outburst Floods From “Hazard Lake”, Yukon Territory, and the Problem of Flood Magnitude Prediction, *Journal of Glaciology*, 28, 3–21, <https://doi.org/10.3189/S0022143000011746>, 1982.
- Clarke, G. K. C.: Hydraulics of subglacial outburst floods: New insights from the Spring–Hutter formulation, *Journal of Glaciology*, 49, 299–313, <https://doi.org/10.3189/172756503781830728>, 2003.
- Conrad, O., Bechtel, B., Bock, M., Dietrich, H., Fischer, E., Gerlitz, L., Wehberg, J., Wichmann, V., and Böhner, J.: System for Automated  
565 Geoscientific Analyses (SAGA) v. 2.1.4, *Geoscientific Model Development*, 8, 1991–2007, <https://doi.org/10.5194/gmd-8-1991-2015>, 2015.
- Cramer, F.: Scientific colour maps: perceptually uniform and colour-vision deficiency friendly, <https://doi.org/10.5281/zenodo.1243862>, 2018.
- Crozier, M. J.: Deciphering the effect of climate change on landslide activity: A review, *Geomorphology*, 124, 260–267,  
570 <https://doi.org/10.1016/j.geomorph.2010.04.009>, 2010.



- Cruden, D. M. and Varnes, D. J.: Landslide Types and Processes, in: Landslides, edited by Turner, A. K. and Schuster, R. L., Transportation Research Board Special Report, pp. 36–75, National Academy of Sciences, Washington, 1996.
- Cuffey, K. M. and Paterson, W. S. B.: The Physics of Glaciers, Elsevier Butterworth Heinemann, Burlington, MA, 4 edn., 2010.
- Delaloye, R., Morard, S., Barboux, C., Abbet, D., Gruber, V., Riedo, M., and Gachet, S.: Rapidly moving rock glaciers in Mattertal, in: 575 Mattertal - ein Tal in Bewegung, edited by Graf, C., pp. 21–31, Eidgenössische Forschungsanstalt für Wald, Schnee und Landschaft (WSL), Birmensdorf, 2013.
- Deline, P., Gruber, S., Delaloye, R., Fischer, L., Geertsema, M., Giardino, M., Hasler, A., Kirkbride, M., Krautblatter, M., Magnin, F., McColl, S., Ravel, L., and Schoeneich, P.: Ice Loss and Slope Stability in High-Mountain Regions, in: Snow and Ice-Related Hazards, Risks, and Disasters, edited by Haeberli, W., Whiteman, C., and Shroder, Jr., J. F., pp. 521–561, Elsevier, Amsterdam, 2015.
- 580 Destro, E., Marra, F., Nikolopoulos, E. I., Zoccatelli, D., Creutin, J. D., and Borga, M.: Spatial estimation of debris flows-triggering rainfall and its dependence on rainfall return period, *Geomorphology*, 278, 269–279, <https://doi.org/10.1016/j.geomorph.2016.11.019>, 2017.
- Dowling, C. A. and Santi, P. M.: Debris flows and their toll on human life: A global analysis of debris-flow fatalities from 1950 to 2011, *Natural Hazards*, 71, 203–227, <https://doi.org/10.1007/s11069-013-0907-4>, 2014.
- Duque, L. F.: Inter-Event Time Definition: R package ‘IETD’, <https://cran.r-project.org/web/packages/IETD/>, last accessed 28 June 2022, 585 2020.
- Ermini, L. and Casagli, N.: Prediction of the behaviour of landslide dams using a geomorphological dimensionless index, *Earth Surface Processes and Landforms*, 28, 31–47, <https://doi.org/10.1002/esp.424>, 2003.
- Escher-Vetter, H.: Energy Balance Calculations for the Ablation Period 1982 at Vernagtferner, Oetztal Alps, *Annals of Glaciology*, 6, 158–160, 1985.
- 590 Evans, S. G. and Delaney, K. B.: Catastrophic Mass Flows in the Mountain Glacial Environment, in: Snow and Ice-Related Hazards, Risks, and Disasters, edited by Haeberli, W., Whiteman, C., and Shroder, Jr., J. F., pp. 563–606, Elsevier, Amsterdam, 2015.
- Fischer, A., Seiser, B., Stocker Waldhuber, M., Mitterer, C., and Abermann, J.: Tracing glacier changes in Austria from the Little Ice Age to the present using a lidar-based high-resolution glacier inventory in Austria, *The Cryosphere*, 9, 753–766, <https://doi.org/10.5194/tc-9-753-2015>, 2015.
- 595 Fleischer, F., Haas, F., Piermattei, L., Pfeiffer, M., Heckmann, T., Altmann, M., Rom, J., Stark, M., Wimmer, M. H., Pfeifer, N., and Becht, M.: Multi-decadal (1953–2017) rock glacier kinematics analysed by high-resolution topographic data in the upper Kaunertal, Austria, *The Cryosphere*, 15, 5345–5369, <https://doi.org/10.5194/tc-15-5345-2021>, 2021.
- Folk, R. L. and Ward, W. C.: Brazos River bar [Texas]; a study in the significance of grain size parameters, *Journal of Sedimentary Research*, 27, 3–26, <https://doi.org/10.1306/74D70646-2B21-11D7-8648000102C1865D>, 1957.
- 600 Fox-Kemper, B., Hewitt, H. T., Xiao, C., Aðalgeirsdóttir, G., Drijfhout, S. S., Edwards, T. L., Golledge, N. R., Hemer, M., Kopp, R. E., Krinner, G., Mix, A., Notz, D., Nowicki, S., Nurhati, I. S., Ruiz, L., Sallée, J.-B., Slangen, A. B. A., and Yu, Y.: Ocean, Cryosphere and Sea Level Change., in: *Climate Change 2021: The Physical Science Basis. Contribution of Working Group I to the Sixth Assessment Report of the Intergovernmental Panel on Climate Change*, edited by Masson-Delmotte, V., Zhai, P., Pirani, A., Connors, S. L., Péan, C., Berger, S., Caud, N., Chen, Y., Goldfarb, L., Gomis, M. I., Huang, M., Leitzell, K., Lonnoy, E., Matthews, J. B. R., Maycock, T. K., 605 Waterfield, T., Yelekçi, O., Yu, R., and Zhou, B., Cambridge University Press, 2021.
- Freeman, T. G.: Calculating catchment area with divergent flow based on a regular grid, *Computers & Geosciences*, 17, 413–422, 1991.
- Frei, C. and Schär, C.: A precipitation climatology of the Alps from high-resolution rain-gauge observations, *International Journal of Climatology*, 18, 873–900, 1998.



- Gallina, V., Torresan, S., Critto, A., Sperotto, A., Glade, T., and Marcomini, A.: A review of multi-risk methodologies for natural hazards: Consequences and challenges for a climate change impact assessment, *Journal of environmental management*, 168, 123–132, <https://doi.org/10.1016/j.jenvman.2015.11.011>, 2016.
- Gariano, S. L. and Guzzetti, F.: Landslides in a changing climate, *Earth-Science Reviews*, 162, 227–252, <https://doi.org/10.1016/j.earscirev.2016.08.011>, 2016.
- Giardino, J. R., Vitek, J. D., and DeMorett, J. L.: A Model of Water Movement in Rock Glaciers and Associated Water Characteristics, in: *Periglacial Geomorphology*, edited by Dixon, J. C. and Abrahams, A. D., pp. 159–184, Wiley, Chichester, 1991.
- Giorgi, F., Torma, C., Coppola, E., Ban, N., Schär, C., and Somot, S.: Enhanced summer convective rainfall at Alpine high elevations in response to climate warming, *Nature Geoscience*, 9, 584–589, <https://doi.org/10.1038/NGEO2761>, 2016.
- Glade, T. and Crozier, M. J.: The Nature of Landslide Hazard Impact, in: *Landslide Hazard and Risk*, edited by Glade, T., Anderson, M., and Crozier, M. J., pp. 43–74, John Wiley & Sons, Chichester, 2005.
- Government of the Province of Tyrol: Digital terrain model, <https://www.data.gv.at/>, last accessed 28 June 2022, CC-BY 4.0, 2021a.
- Government of the Province of Tyrol: Current and historical orthoimagery of Tyrol, <https://www.data.gv.at/>, last accessed 28 June 2022, CC-BY 4.0, 2021b.
- GRASS Development Team: Geographic Resources Analysis Support System (GRASS), <https://grass.osgeo.org>, last accessed 28 June 2022, 2022.
- Greuell, W. and Oerlemans, J.: Energy Balance Calculations on and near Hintereisferner (Austria) and an Estimate of the Effect of Greenhouse Warming on Ablation, in: *Glacier Fluctuations and Climatic Change*, edited by Oerlemans, J., *Glaciology and Quaternary Geology*, pp. 305–323, Springer, Dordrecht, 1989.
- Greuell, W., van den Broeke, M., Knap, W., Reijmer, C., Smeets, P., and Struijk, I.: PASTEX (PASTERze EXperiment): Field report on a glacio-meteorological experiment on the Pasterze (Austria).
- Greuell, W., Knap, W. H., and Smeets, P. C.: Elevational changes in meteorological variables along a midlatitude glacier during summer, *Journal of Geophysical Research*, 102, 25 941–25 954, <https://doi.org/10.1029/97JD02083>, 1997.
- Groh, T. and Blöthe, J. H.: Rock Glacier Kinematics in the Kaunertal, Ötztal Alps, Austria, *Geosciences*, 9, 373, <https://doi.org/10.3390/geosciences9090373>, 2019.
- Guzzetti, F., Peruccacci, S., Rossi, M., and Stark, C. P.: Rainfall thresholds for the initiation of landslides in central and southern Europe, *Meteorology and Atmospheric Physics*, 98, 239–267, <https://doi.org/10.1007/s00703-007-0262-7>, 2007.
- Haeberli, W.: Frequency and Characteristics of Glacier Floods in the Swiss Alps, *Annals of Glaciology*, 4, 85–90, <https://doi.org/10.3189/S0260305500005280>, 1983.
- Haeberli, W. and Vonder Mühl, D.: On the characteristics and possible origins of ice in rock glacier permafrost, *Zeitschrift für Geomorphologie, Supplementary Issues*, 104, 43–57, 1996.
- Haeberli, W. and Whiteman, C.: Snow and Ice-Related Hazards, Risks, and Disasters: A General Framework, in: *Snow and Ice-Related Hazards, Risks, and Disasters*, edited by Haeberli, W., Whiteman, C., and Shroder, Jr., J. F., pp. 1–34, Elsevier, Amsterdam, 2015.
- Haeberli, W., Käab, A., Vonder Mühl, D., and Teyssie, P.: Prevention of outburst floods from periglacial lakes at Grubengletscher, Valais, Swiss Alps, *Journal of Glaciology*, 47, 111–122, 2001.
- Haiden, T., Kann, A., Wittmann, C., Pistotnik, G., Bica, B., and Gruber, C.: The Integrated Nowcasting through Comprehensive Analysis (INCA) System and Its Validation over the Eastern Alpine Region, *Weather and Forecasting*, 26, 166–183, <https://doi.org/10.1175/2010WAF2222451.1>, 2011.



- Haque, U., Blum, P., da Silva, P. F., Andersen, P., Pilz, J., Chalov, S. R., Malet, J.-P., Auflič, M. J., Andres, N., Poyiadji, E., Lamas, P. C., Zhang, W., Peshevski, I., Pétursson, H. G., Kurt, T., Dobrev, N., García-Davalillo, J. C., Halkia, M., Ferri, S., Gaprindashvili, G., Engström, J., and Keellings, D.: Fatal landslides in Europe, *Landslides*, 13, 1545–1554, <https://doi.org/10.1007/s10346-016-0689-3>, 2016.
- 650 Haque, U., da Silva, P. F., Devoli, G., Pilz, J., Zhao, B., Khaloua, A., Wilopo, W., Andersen, P., Lu, P., Lee, J., Yamamoto, T., Keellings, D., Wu, J.-H., and Glass, G. E.: The human cost of global warming: Deadly landslides and their triggers (1995-2014), *Science of the Total Environment*, 682, 673–684, <https://doi.org/10.1016/j.scitotenv.2019.03.415>, 2019.
- Hayashi, M.: Alpine Hydrogeology: The Critical Role of Groundwater in Sourcing the Headwaters of the World, *Ground Water*, 58, 498–510, <https://doi.org/10.1111/gwat.12965>, 2020.
- 655 Hiebl, J. and Frei, C.: Daily temperature grids for Austria since 1961—concept, creation and applicability, *Theoretical and Applied Climatology*, 124, 161–178, <https://doi.org/10.1007/s00704-015-1411-4>, 2016.
- Hiebl, J. and Frei, C.: Daily precipitation grids for Austria since 1961—development and evaluation of a spatial dataset for hydroclimatic monitoring and modelling, *Theoretical and Applied Climatology*, 132, 327–345, <https://doi.org/10.1007/s00704-017-2093-x>, 2018.
- Hirsch, R. M. and Slack, J. R.: A Nonparametric Trend Test for Seasonal Data With Serial Dependence, *Water Resources Research*, 20, 660 727–732, <https://doi.org/10.1029/WR020i006p00727>, 1984.
- Hirsch, R. M., Slack, J. R., and Smith, R. A.: Techniques of Trend Analysis for Monthly Water Quality Data, *Water Resources Research*, 18, 107–121, 1982.
- Hock, R.: Glacier melt: a review of processes and their modelling, *Progress in Physical Geography*, 29, 263–391, 2005.
- Hock, R., Rasul, G., Adler, C., Cáceres, B., Gruber, S., Hirabayashi, Y., Jackson, M., Käab, A., Kang, S., Kutuzov, S., Milner, A., Molau, 665 U., Morin, S., Orlove, B., and Steltzer, H.: High Mountain Areas, in: *IPCC Special Report on the Ocean and Cryosphere in a Changing Climate*, edited by Intergovernmental Panel on Climate Change, pp. 131–202, 2019.
- Hofierka, J., Suri, M., and Huld, T.: Solar irradiance and irradiation model: GRASS GIS 8.0 module ‘r.sun’, <https://grass.osgeo.org/grass80/manuals/r.sun.html>, last accessed 28 June 2022, 2007.
- Hoinkes, G. and Thöni, M.: Evolution of the Ötztal-Stubai, Scarl-Campo and Ulten Basement Units, in: *Pre-Mesozoic Geology in the Alps*, 670 edited by Raumer, J. F. and Neubauer, F., pp. 485–494, Springer Berlin Heidelberg, Berlin, Heidelberg, 1993.
- Huggel, C., Haeberli, W., Käab, A., Bieri, D., and Richardson, S.: An assessment procedure for glacial hazards in the Swiss Alps, *Canadian Geotechnical Journal*, 41, 1068–1083, <https://doi.org/10.1139/t04-053>, 2004.
- Hungr, O.: Classification and terminology, in: *Debris-flow Hazards and Related Phenomena*, edited by Jakob, M. and Hungr, O., pp. 9–24, Springer-Verlag Berlin Heidelberg, 2005.
- 675 Hungr, O., Leroueil, S., and Picarelli, L.: The Varnes classification of landslide types, an update, *Landslides*, 11, 167–194, 2014.
- Hutchinson, J. N. and Bhandari, R. K.: Undrained Loading, A Fundamental Mechanism of Mudflows and other Mass Movements, *Géotechnique*, 21, 353–358, <https://doi.org/10.1680/geot.1971.21.4.353>, 1971.
- Hydrological Service of Tyrol: Hydrological summary, <https://www.tirol.gv.at/umwelt/wasserwirtschaft/wasserkreislauf/hydrologische-uebersichten/>, last accessed 28 June 2022, 2019.
- 680 Ikeda, A. and Matsuoka, N.: Pebbly versus bouldery rock glaciers: Morphology, structure and processes, *Geomorphology*, 73, 279–296, <https://doi.org/10.1016/j.geomorph.2005.07.015>, 2006.
- Ikeda, A., Matsuoka, N., and Käab, A.: Fast deformation of perennially frozen debris in a warm rock glacier in the Swiss Alps: An effect of liquid water, *Journal of Geophysical Research*, 113, <https://doi.org/10.1029/2007JF000859>, 2008.



- International Organization for Standardization: ISO 14688-1:2017 Geotechnical investigation and testing - Identification and classification  
685 of soil - Part 1: Identification and description, 2017.
- Isotta, F. A., Frei, C., Weilguni, V., Perčec Tadić, M., Lassègues, P., Rudolf, B., Pavan, V., Cacciamani, C., Antolini, G., Ratto, S. M., Munari, M., Micheletti, S., Bonati, V., Lussana, C., Ronchi, C., Panettieri, E., Marigo, G., and Vertačnik, G.: The climate of daily precipitation in the Alps: Development and analysis of a high-resolution grid dataset from pan-Alpine rain-gauge data, *International Journal of Climatology*, 34, 1657–1675, <https://doi.org/10.1002/joc.3794>, 2014.
- 690 Iverson, R. M.: The physics of debris flows, *Reviews of Geophysics*, 35, 245–296, 1997.
- Iverson, R. M.: Debris-flow mechanics, in: *Debris-flow Hazards and Related Phenomena*, edited by Jakob, M. and Hungr, O., pp. 105–134, Springer-Verlag Berlin Heidelberg, 2005.
- Iverson, R. M. and LaHusen, R. G.: Dynamic Pore-Pressure Fluctuations in Rapidly Shearing Granular Materials, *Science*, 246, 796–799, 1989.
- 695 Iverson, R. M. and Major, J. J.: Groundwater Seepage Vectors and the Potential for Hillslope Failure and Debris Flow Mobilization, *Water Resources Research*, 22, 1543–1548, <https://doi.org/10.1029/WR022i01p01543>, 1986.
- Iverson, R. M., Reid, M. E., and LaHusen, R. G.: Debris-flow mobilization from landslides, *Annual Review of Earth and Planetary Sciences*, 25, 85–138, <https://doi.org/10.1146/annurev.earth.25.1.85>, 1997.
- Jakob, M. and Hungr, O.: Introduction, in: *Debris-flow Hazards and Related Phenomena*, edited by Jakob, M. and Hungr, O., pp. 1–8,  
700 Springer-Verlag Berlin Heidelberg, 2005.
- Jakob, M., Owen, T., and Simpson, T.: A regional real-time debris-flow warning system for the District of North Vancouver, Canada, *Landslides*, 9, 165–178, <https://doi.org/10.1007/s10346-011-0282-8>, 2012.
- Johnson, K. A. and Sitar, N.: Hydrologic conditions leading to debris-flow initiation, *Canadian Geotechnical Journal*, 27, 789–801, <https://doi.org/10.1139/t90-092>, 1990.
- 705 Johnson, P. G.: Rock glacier types and their drainage systems, Grizzly Creek, Yukon Territory, *Canadian Journal of Earth Sciences*, 15, 1496–1507, 1978.
- Johnson, P. G.: Micro-relief on a Rock Glacier, Dalton Range, Yukon, Canada, *Permafrost and Periglacial Processes*, 3, 41–47, 1992.
- Jones, D. B., Harrison, S., and Anderson, K.: Mountain glacier-to-rock glacier transition, *Global and Planetary Change*, 181, 102 999, <https://doi.org/10.1016/j.gloplacha.2019.102999>, 2019a.
- 710 Jones, D. B., Harrison, S., Anderson, K., and Whalley, W. B.: Rock glaciers and mountain hydrology: A review, *Earth-Science Reviews*, 193, 66–90, <https://doi.org/10.1016/j.earscirev.2019.04.001>, 2019b.
- Kääb, A. and Haeberli, W.: Evolution of a High-Mountain Thermokarst Lake in the Swiss Alps, *Arctic, Antarctic, and Alpine Research*, 33, 385–390, 2001.
- Kääb, A., Frauenfelder, R., and Roer, I.: On the response of rockglacier creep to surface temperature increase, *Global and Planetary Change*,  
715 56, 172–187, 2007.
- Kainz, S.: *Characterizing Groundwater Flow Dynamics and Storage Capacity in an Active Rock Glacier*, Springer Fachmedien, Wiesbaden, <https://doi.org/10.1007/978-3-658-37073-2>, 2022.
- Kappes, M. S., Keiler, M., von Elverfeldt, K., and Glade, T.: Challenges of analyzing multi-hazard risk: A review, *Natural Hazards*, 64, 1925–1958, <https://doi.org/10.1007/s11069-012-0294-2>, 2012.
- 720 Kenner, R., Pruessner, L., Beutel, J., Limpach, P., and Phillips, M.: How rock glacier hydrology, deformation velocities and ground temperatures interact: Examples from the Swiss Alps, *Permafrost and Periglacial Processes*, 31, 3–14, <https://doi.org/10.1002/ppp.2023>, 2020.



- Kerschner, H.: Zeugen der Klimageschichte im oberen Radurschltal: Alte Gletscherstände und Blockgletscher in der Umgebung des Hohenzollernhauses, *Zeitschrift des Deutschen und Österreichischen Alpenvereins*, 107, 23–27, 1982.
- Klein Tank, A. M. G., Zwiers, F. W., and Zhang, X.: Guidelines on analysis of extremes in a changing climate in support of informed decisions for adaptation, no. 72 in *World Climate Data and Monitoring Programme (WCDMP)*, World Meteorological Organization, Geneva, 2009.
- 725 Klok, E. J. and Oerlemans, J.: Model study of the spatial distribution of the energy and mass balance of Morteratschgletscher, Switzerland, *Journal of Glaciology*, 48, 505–518, <https://doi.org/10.3189/172756502781831133>, 2002.
- Knight, J., Harrison, S., and Jones, D. B.: Rock glaciers and the geomorphological evolution of deglaciating mountains, *Geomorphology*, 324, 14–24, <https://doi.org/10.1016/j.geomorph.2018.09.020>, 2019.
- 730 Kofler, C., Mair, V., Gruber, S., Todisco, M. C., Nettleton, I., Steger, S., Zebisch, M., Schneiderbauer, S., and Comiti, F.: When do rock glacier fronts fail? Insights from two case studies in South Tyrol (Italian Alps), *Earth Surface Processes and Landforms*, <https://doi.org/10.1002/esp.5099>, 2021.
- Krainer, K. and Mostler, W.: Hydrology of Active Rock Glaciers: Examples from the Austrian Alps, *Arctic, Antarctic, and Alpine Research*, 34, 142–149, <https://doi.org/10.1080/15230430.2002.12003478>, 2002.
- 735 Krainer, K. and Ribis, M.: A Rock Glacier Inventory of the Tyrolean Alps (Austria), *Austrian Journal of Earth Sciences*, 105, 32–47, 2012.
- Krainer, K., Lang, K., and Hausmann, H.: Active Rock Glaciers at Croda Rossa/Hohe Gaisl, Eastern Dolomites (Alto Adige/South Tyrol, Northern Italy), *Geogr. Fis. Dinam. Quat.*, pp. 25–36, 2010.
- Krainer, K., Mussner, L., Behm, M., and Hausmann, H.: Multi-disciplinary investigation of an active rock glacier in the Sella Group (Dolomites; Northern Italy), *Austrian Journal of Earth Sciences*, 105, 48–62, 2012.
- 740 Krainer, K., Bressan, D., Dietre, B., Haas, J. N., Hajdas, I., Lang, K., Mair, V., Nickus, U., Reidl, D., Thies, H., and Tonidandel, D.: A 10,300-year-old permafrost core from the active rock glacier Lazaun, southern Ötztal Alps (South Tyrol, northern Italy), *Quaternary Research*, 83, 324–335, <https://doi.org/10.1016/j.yqres.2014.12.005>, 2015.
- Kummert, M. and Delaloye, R.: Mapping and quantifying sediment transfer between the front of rapidly moving rock glaciers and torrential gullies, *Geomorphology*, 309, 60–76, <https://doi.org/10.1016/j.geomorph.2018.02.021>, 2018.
- 745 Kummert, M., Delaloye, R., and Braillard, L.: Erosion and sediment transfer processes at the front of rapidly moving rock glaciers: Systematic observations with automatic cameras in the western Swiss Alps, *Permafrost and Periglacial Processes*, 29, 21–33, <https://doi.org/10.1002/ppp.1960>, 2018.
- Lugon, R. and Stoffel, M.: Rock-glacier dynamics and magnitude–frequency relations of debris flows in a high-elevation watershed: Riti-graben, Swiss Alps, *Global and Planetary Change*, 73, 202–210, <https://doi.org/10.1016/j.gloplacha.2010.06.004>, 2010.
- 750 Major, J. J.: Experimental studies of deposition by debris flows: process, characteristics of deposits, and effects of pore-fluid pressure, Dissertation, University of Washington, Seattle, 1996.
- Major, J. J., Iverson, R. M., McTigue, D. F., Macias, S., and Fiedorowicz, B. K.: Geotechnical properties of debris-flow sediments and slurries, in: *Debris-flow hazards mitigation: mechanics, prediction, and assessment*, edited by Chen, C.-I., pp. 249–259, American Society of Civil Engineers, New York, NY, 1997.
- 755 Marcer, M., Serrano, C., Brenning, A., Bodin, X., Goetz, J., and Schoeneich, P.: Evaluating the destabilization susceptibility of active rock glaciers in the French Alps, *The Cryosphere*, 13, 141–155, <https://doi.org/10.5194/tc-13-141-2019>, 2019.
- Marcer, M., Ringsø Nielsen, S., Ribeyre, C., Kummert, M., Duvillard, P.-A., Schoeneich, P., Bodin, X., and Genuite, K.: Investigating the slope failures at the Lou rock glacier front, French Alps, *Permafrost and Periglacial Processes*, 31, 15–30, <https://doi.org/10.1002/ppp.2035>, 2020.



- 760 Marcer, M., Cicoira, A., Cusicanqui, D., Bodin, X., Echelard, T., Obregon, R., and Schoeneich, P.: Rock glaciers throughout the French Alps accelerated and destabilised since 1990 as air temperatures increased, *Communications Earth & Environment*, 2, 383, <https://doi.org/10.1038/s43247-021-00150-6>, 2021.
- Marchetto, A.: Mann-Kendall Test, Seasonal and Regional Kendall Tests: R package ‘rkt’, <https://cran.r-project.org/web/packages/rkt/>, last accessed 28 June 2022, 2021.
- 765 Marra, F.: Rainfall thresholds for landslide occurrence: Systematic underestimation using coarse temporal resolution data, *Natural Hazards*, 95, 883–890, <https://doi.org/10.1007/s11069-018-3508-4>, 2019.
- Marra, F., Nikolopoulos, E. I., Creutin, J. D., and Borga, M.: Radar rainfall estimation for the identification of debris-flow occurrence thresholds, *Journal of Hydrology*, 519, 1607–1619, <https://doi.org/10.1016/j.jhydrol.2014.09.039>, 2014.
- Marra, F., Nikolopoulos, E. I., Creutin, J. D., and Borga, M.: Space–time organization of debris flows-triggering rainfall and its effect on  
770 the identification of the rainfall threshold relationship, *Journal of Hydrology*, 541, 246–255, <https://doi.org/10.1016/j.jhydrol.2015.10.010>, 2016.
- Matiu, M., Crespi, A., Bertoldi, G., Carmagnola, C. M., Marty, C., Morin, S., Schöner, W., Cat Berro, D., Chiogna, G., de Gregorio, L., Kotlarski, S., Majone, B., Resch, G., Terzago, S., Valt, M., Beozzo, W., Cianfarra, P., Gouttevin, I., Marcolini, G., Notarnicola, C., Petitta, M., Scherrer, S. C., Strasser, U., Winkler, M., Zebisch, M., Cicogna, A., Cremonini, R., Debernardi, A., Faletto, M., Gaddo, M.,  
775 Giovannini, L., Mercalli, L., Soubeyroux, J.-M., Sušnik, A., Trenti, A., Urbani, S., and Weigluni, V.: Observed snow depth trends in the European Alps: 1971 to 2019, *The Cryosphere*, 15, 1343–1382, <https://doi.org/10.5194/tc-15-1343-2021>, 2021.
- Mölg, N., Huggel, C., Herold, T., Storck, F., Allen, S., Haerberli, W., Schaub, Y., and Odermatt, D.: Inventory and evolution of glacial lakes since the Little Ice Age: Lessons from the case of Switzerland, *Earth Surface Processes and Landforms*, 46, 2551–2564, <https://doi.org/10.1002/esp.5193>, 2021.
- 780 Moser, M.: GEOFAST 1:50 000. Zusammenstellung ausgewählter Archivunterlagen der Geologischen Bundesanstalt: Blatt 172 Weißkugel, 2012.
- Nikolopoulos, E. I., Crema, S., Marchi, L., Marra, F., Guzzetti, F., and Borga, M.: Impact of uncertainty in rainfall estimation on the identification of rainfall thresholds for debris flow occurrence, *Geomorphology*, 221, 286–297, <https://doi.org/10.1016/j.geomorph.2014.06.015>, 2014.
- 785 Nikolopoulos, E. I., Borga, M., Creutin, J. D., and Marra, F.: Estimation of debris flow triggering rainfall: Influence of rain gauge density and interpolation methods, *Geomorphology*, 243, 40–50, <https://doi.org/10.1016/j.geomorph.2015.04.028>, 2015a.
- Nikolopoulos, E. I., Borga, M., Marra, F., Crema, S., and Marchi, L.: Debris flows in the eastern Italian Alps: Seasonality and atmospheric circulation patterns, *Natural Hazards and Earth System Sciences*, 15, 647–656, <https://doi.org/10.5194/nhess-15-647-2015>, 2015b.
- Nye, J. F.: Water Flow in Glaciers: Jökulhlaups, Tunnels and Veins, *Journal of Glaciology*, 17, 181–207,  
790 <https://doi.org/10.3189/S002214300001354X>, 1976.
- Oerlemans, J.: Analysis of a 3 year meteorological record from the ablation zone of Morteratschgletscher, Switzerland: Energy and mass balance, *Journal of Glaciology*, 46, 571–579, <https://doi.org/10.3189/172756500781832657>, 2000.
- Oerlemans, J. and Klok, E. J.: Energy Balance of a Glacier Surface: Analysis of Automatic Weather Station Data from the Morteratschgletscher, Switzerland, Arctic, Antarctic, and Alpine Research, 34, 477–485, <https://doi.org/10.1080/15230430.2002.12003519>,  
795 2002.
- Oerlemans, J., Giesen, R. H., and van den Broeke, M. R.: Retreating alpine glaciers: Increased melt rates due to accumulation of dust (Vadret da Morteratsch, Switzerland), *Journal of Glaciology*, 55, 729–736, <https://doi.org/10.3189/002214309789470969>, 2009.



- Olefs, M., Schöner, W., Suklitsch, M., Wittmann, C., Niedermoser, B., Neururer, A., and Wurzer, A.: SNOWGRID – A new operational snow cover model in Austria, in: *Proceedings of International Snow Science Workshop, Grenoble-Chamonix, 7-11 October 2013: a merging of theory and practice*, edited by Bouvet, F. N., Ruand, Y., and Lambert, R., pp. 38–45, 2013.
- Olefs, M., Baumgartner, D. J., Obleitner, F., Bichler, C., Foelsche, U., Pietsch, H., Rieder, H. E., Weihs, P., Geyer, F., Haiden, T., and Schöner, W.: The Austrian radiation monitoring network ARAD – best practice and added value, *Atmospheric Measurement Techniques*, 9, 1513–1531, <https://doi.org/10.5194/amt-9-1513-2016>, 2016.
- Olefs, M., Koch, R., Schöner, W., and Marke, T.: Changes in Snow Depth, Snow Cover Duration, and Potential Snowmaking Conditions in Austria, 1961–2020—A Model Based Approach, *Atmosphere*, 11, 1330, <https://doi.org/10.3390/atmos11121330>, 2020.
- Pack, R. T.: Application of airborne and spaceborne remote sensing methods, in: *Debris-flow Hazards and Related Phenomena*, edited by Jakob, M. and Hungr, O., pp. 275–290, Springer-Verlag Berlin Heidelberg, 2005.
- Patton, A. I., Rathburn, S. L., and Capps, D. M.: Landslide response to climate change in permafrost regions, *Geomorphology*, 340, 116–128, <https://doi.org/10.1016/j.geomorph.2019.04.029>, 2019.
- Peruccacci, S., Brunetti, M. T., Luciani, S., Vennari, C., and Guzzetti, F.: Lithological and seasonal control on rainfall thresholds for the possible initiation of landslides in central Italy, *Geomorphology*, 139–140, 79–90, <https://doi.org/10.1016/j.geomorph.2011.10.005>, 2012.
- Petley, D.: Global patterns of loss of life from landslides, *Geology*, 40, 927–930, <https://doi.org/10.1130/G33217.1>, 2012.
- Potter, N.: Ice-Cored Rock Glacier, Galena Creek, Northern Absaroka Mountains, Wyoming, *Geological Society of America Bulletin*, 83, 3025, [https://doi.org/10.1130/0016-7606\(1972\)83\[3025:IRGGCN\]2.0.CO;2](https://doi.org/10.1130/0016-7606(1972)83[3025:IRGGCN]2.0.CO;2), 1972.
- R Core Team: R: A language and environment for statistical computing, <http://www.R-project.org>, last accessed 28 June 2022, 2022.
- Rajczak, J. and Schär, C.: Projections of Future Precipitation Extremes Over Europe: A Multimodel Assessment of Climate Simulations, *Journal of Geophysical Research: Atmospheres*, 122, 10,773–10,800, <https://doi.org/10.1002/2017JD027176>, 2017.
- Ranasinghe, R., Ruane, A. C., Vautard, R., Arnell, N., Coppola, E., Cruz, F. A., Dessai, S., Islam, A. S., Rahimi, M., Ruiz Carrascal, D., Sillmann, J., Sylla, M. B., Tebaldi, C., Wang, W., and Zaaboul, R.: Climate Change Information for Regional Impact and for Risk Assessment, in: *Climate Change 2021: The Physical Science Basis. Contribution of Working Group I to the Sixth Assessment Report of the Intergovernmental Panel on Climate Change*, edited by Masson-Delmotte, V., Zhai, P., Pirani, A., Connors, S. L., Péan, C., Berger, S., Caud, N., Chen, Y., Goldfarb, L., Gomis, M. I., Huang, M., Leitzell, K., Lonnoy, E., Matthews, J. B. R., Maycock, T. K., Waterfield, T., Yelekçi, O., Yu, R., and Zhou, B., Cambridge University Press, 2021.
- Rebetez, M., Lugon, R., and Baeriswyl, P.-A.: Climatic change and debris flows in high mountain regions: the case study of the Ritigraben Torrent (Swiss Alps), *Climatic Change*, 36, 371–389, 1997.
- Reichenbach, P., Rossi, M., Malamud, B. D., Mihir, M., and Guzzetti, F.: A review of statistically-based landslide susceptibility models, *Earth-Science Reviews*, 180, 60–91, <https://doi.org/10.1016/j.earscirev.2018.03.001>, 2018.
- Ribis, M.: *Geologisch-hydrogeologische und hydrochemische Untersuchungen in Permafrostbereichen der Ötztaler Alpen (Tirol, Österreich)*, Dissertation, Leopold-Franzens-Universität, Innsbruck, 2017.
- Roer, I., Haerberli, W., Avian, M., Kaufmann, V., Delaloye, R., Lambiel, C., and Kääh, A.: Observations and Considerations on Destabilizing Active Rock Glaciers in the European Alps, in: *Proceedings of the 9th International Conference on Permafrost*, edited by Kane, D. L. and Hinkel, K. M., pp. 1505–1510, University of Alaska Fairbanks, Fairbanks, 2008.
- Sassa, K. and Wang, G. h.: Mechanism of landslide-triggered debris flows: Liquefaction phenomena due to the undrained loading of torrent deposits, in: *Debris-flow Hazards and Related Phenomena*, edited by Jakob, M. and Hungr, O., pp. 81–104, Springer-Verlag Berlin Heidelberg, 2005.



- Savage, W. and Baum, R.: Instability of steep slopes, in: Debris-flow Hazards and Related Phenomena, edited by Jakob, M. and Hungr, O., pp. 53–80, Springer-Verlag Berlin Heidelberg, 2005.
- Schaub, Y.: Outburst floods from high-mountain lakes: risk analysis of cascading processes under present and future conditions, Dissertation, Universität Zürich, Zürich, 2015.
- 840 Schauwecker, S., Gascón, E., Park, S., Ruiz-Villanueva, V., Schwarb, M., Sempere-Torres, D., Stoffel, M., Vitolo, C., and Rohrer, M.: Anticipating cascading effects of extreme precipitation with pathway schemes - Three case studies from Europe, *Environment international*, 127, 291–304, <https://doi.org/10.1016/j.envint.2019.02.072>, 2019.
- Scherler, M., Schneider, S., Hoelzle, M., and Hauck, C.: A two-sided approach to estimate heat transfer processes within the active layer of the Murtèl–Corvatsch rock glacier, *Earth Surface Dynamics*, 2, 141–154, <https://doi.org/10.5194/esurf-2-141-2014>, 2014.
- 845 Schlögl, M. and Matulla, C.: Potential future exposure of European land transport infrastructure to rainfall-induced landslides throughout the 21st century, *Natural Hazards and Earth System Sciences*, 18, 1121–1132, <https://doi.org/10.5194/nhess-18-1121-2018>, 2018.
- Schmid, S. M., Fügenschuh, B., Kissling, E., and Schuster, R.: Tectonic map and overall architecture of the Alpine orogen, *Eclogae Geologicae Helvetiae*, 97, 93–117, 2004.
- Sen, P. K.: Estimates of the Regression Coefficient Based on Kendall’s Tau, *Journal of the American Statistical Association*, 63, 1379–1389, 1968.
- 850 Sentinel Hub: Modified Sentinel-2 multi-spectral satellite data, produced from European Space Agency remote sensing data provided by Copernicus, images processed by Sentinel Hub, <https://www.sentinel-hub.com/>, last accessed 28 June 2022, 2020.
- Sidle, R. C.: Shallow groundwater fluctuations in unstable hillslopes of coastal Alaska, *Zeitschrift für Gletscherkunde und Glazialgeologie*, 20, 79–95, 1984.
- 855 Soeters, R. and van Westen, C. J.: Slope Instability Recognition, Analysis, and Zonation, in: Landslides, edited by Turner, A. K. and Schuster, R. L., Transportation Research Board Special Report, pp. 129–177, National Academy of Sciences, Washington, 1996.
- Spring, U. and Hutter, K.: Conduit flow of a fluid through its solid phase and its application to intraglacial channel flow, *Int. J. Eng. Sci.*, 20, 327–363, 1981a.
- Spring, U. and Hutter, K.: Numerical studies of Jökulhlaups, *Cold Regions Science and Technology*, 4, 227–244, 1981b.
- 860 [https://doi.org/10.1016/0165-232X\(81\)90006-9](https://doi.org/10.1016/0165-232X(81)90006-9), 1981b.
- Springman, S. M., Arenson, L. U., Yamamoto, Y., Maurer, H., Kos, A., Buchli, T., and Derungs, G.: Multidisciplinary investigations on three rock glaciers in the swiss alps: Legacies and future perspectives, *Geografiska Annaler: Series A, Physical Geography*, 94, 215–243, <https://doi.org/10.1111/j.1468-0459.2012.00464.x>, 2012.
- Stoffel, M. and Huggel, C.: Effects of climate change on mass movements in mountain environments, *Progress in Physical Geography*, 36, 421–439, <https://doi.org/10.1177/0309133312441010>, 2012.
- 865 Tenthorey, G.: Perennial névés and the hydrology of rock glaciers, *Permafrost and Periglacial Processes*, 3, 247–252, <https://doi.org/10.1002/ppp.3430030313>, 1992.
- Theil, H.: A rank-invariant method of linear and polynomial regression analysis, *Koninklijke Nederlandse Akademie Van Wetenschappen Proceedings*, 53, 386–392, 521–525, 1397–1412, 1950.
- 870 Turner, A. K.: Colluvium and Talus, in: Landslides, edited by Turner, A. K. and Schuster, R. L., Transportation Research Board Special Report, pp. 525–554, National Academy of Sciences, Washington, 1996.
- van de Wal, R. S. W., Oerlemans, J., and van der Hage, J. C.: A study of ablation variations on the tongue of Hintereisferner, Austrian Alps, *Journal of Glaciology*, 38, 319–324, <https://doi.org/10.3189/S0022143000002203>, 1992.



- Varnes, D. J.: Slope Movement Types and Processes, in: Landslides, edited by Schuster, R. L., Krizek, R. J., and National Research Council, 875 Special Report, pp. 12–33, Transportation Research Board and National Academy of Sciences, Washington, D.C., 1978.
- Vonder Mühlh, D. S., Arenson, L. U., and Springman, S. M.: Temperature conditions in two Alpine rock glaciers, in: Proceedings of the 8th International Conference on Permafrost, edited by Phillips, M., Springman, S. M., and Arenson, L. U., pp. 1195–1200, Balkema, Lisse, 2003.
- Wagner, T., Pleschberger, R., Kainz, S., Ribis, M., Kellerer-Pirklbauer, A., Krainer, K., Philippitsch, R., and Winkler, G.: The first consistent inventory of rock glaciers and their hydrological catchments of the Austrian Alps, Austrian Journal of Earth Sciences, 113, 1–23, 880 <https://doi.org/10.17738/ajes.2020.0001>, 2020.
- Wagner, T., Kainz, S., Helfricht, K., Fischer, A., Avian, M., Krainer, K., and Winkler, G.: Assessment of liquid and solid water storage in rock glaciers versus glacier ice in the Austrian Alps, Science of the Total Environment, 800, 149593, <https://doi.org/10.1016/j.scitotenv.2021.149593>, 2021a.
- 885 Wagner, T., Kainz, S., Krainer, K., and Winkler, G.: Storage–discharge characteristics of an active rock glacier catchment in the Innere Ölgrube, Austrian Alps, Hydrological Processes, 35, 42, <https://doi.org/10.1002/hyp.14210>, 2021b.
- Wahrhaftig, C. and Cox, A.: Rock Glaciers in the Alaska Range, Geological Society of America Bulletin, 70, 383, [https://doi.org/10.1130/0016-7606\(1959\)70\[383:RGITAR\]2.0.CO;2](https://doi.org/10.1130/0016-7606(1959)70[383:RGITAR]2.0.CO;2), 1959.
- Walder, J. S. and Costa, J. E.: Outburst floods from glacier-dammed lakes: The effect of mode of lake drainage on flood magnitude, Earth 890 Surface Processes and Landforms, 21, 701–723, [https://doi.org/10.1002/\(SICI\)1096-9837\(199608\)21:8<701::AID-ESP615>3.0.CO;2-2](https://doi.org/10.1002/(SICI)1096-9837(199608)21:8<701::AID-ESP615>3.0.CO;2-2), 1996.
- Werder, M. A., Bauder, A., Funk, M., and Keusen, H.-R.: Hazard assessment investigations in connection with the formation of a lake on the tongue of Unterer Grindelwaldgletscher, Bernese Alps, Switzerland, Natural Hazards and Earth System Sciences, 10, 227–237, <https://doi.org/10.5194/nhess-10-227-2010>, 2010.
- 895 White, S. E.: Rock Glacier Studies in the Colorado Front Range, 1961 to 1968, Arctic and Alpine Research, 3, 43–64, 1971.
- Wieczorek, G. F.: Landslide Triggering Mechanisms, in: Landslides, edited by Turner, A. K. and Schuster, R. L., Transportation Research Board Special Report, pp. 76–90, National Academy of Sciences, Washington, 1996.
- Wieczorek, G. F. and Glade, T.: Climatic factors influencing occurrence of debris flows, in: Debris-flow Hazards and Related Phenomena, edited by Jakob, M. and Hungr, O., pp. 325–362, Springer-Verlag Berlin Heidelberg, 2005.
- 900 Wieczorek, G. F. and Guzzetti, F.: A review of rainfall thresholds for triggering landslides, in: Mediterranean Storms, edited by European Geosciences Union, pp. 407–414, Editoriale Bios, Cosenza, Italy, 2000.
- Willis, I. C., Arnold, N. S., and Brock, B. W.: Effect of snowpack removal on energy balance, melt and runoff in a small supraglacial catchment, Hydrological Processes, 16, 2721–2749, <https://doi.org/10.1002/hyp.1067>, 2002.
- Winkler, G., Wagner, T., Krainer, K., Ribis, M., and Hergarten, S.: Hydrogeology of Rock Glaciers - Storage Capacity and Drainage Dynamics 905 - An Overview, in: Novel methods and results of landscape research in Europe, Central Asia and Siberia, edited by Sychev, V. G. and Mueller, L., pp. 329–334, FGBNU VNII agrochimii, Moskau, 2018.
- Žebre, M., Colucci, R. R., Giorgi, F., Glasser, N. F., Racoviteanu, A. E., and Del Gobbo, C.: 200 years of equilibrium-line altitude variability across the European Alps (1901–2100), Climate Dynamics, 56, 1183–1201, <https://doi.org/10.1007/s00382-020-05525-7>, 2021.